Cold-associated mammokines preserve adipocyte identity

Luis C. Santos[1,7], Douglas Arneson[2,4,7], Karthickeyan Chella Krishnan[3], In Sook Ahn[4], Graciel Diamante[4], Ingrid Cely[4], Atul J. Butte[2,5,6], Aldons J. Lusis[3], Xia Yang[4] , and Prashant Rajbhandari[1, 8]

[1]Diabetes, Obesity, and Metabolism Institute, Icahn School of Medicine at Mount Sinai, New York, NY USA
[2]Bakar Computational Health Sciences Institute**,** University of California, San Francisco, CA USA
[3]Department of Medicine/Division of Cardiology and Department of Human Genetics,
[4]Department of Integrative Biology and Physiology and Bioinformatics Interdepartmental Program, University of California, Los Angeles, CA USA
[5]Department of Pediatrics, University of California, San Francisco, CA, USA
[6]Center for Data-Driven Insights and Innovation, University of California Health, Oakland, CA, USA

[7]Equal Contribution

[8]Corresponding author:

Prashant Rajbhandari PhD
Diabetes, Obesity, and Metabolism Institute
Department of Endocrinology and Bone Disease
Icahn School of Medicine at Mount Sinai
1 Gustave L. Levy Place
New York, NY 10029 USA
Office (212) 659-8653
E-mail: prashant.rajbhandari@mssm.edu

Main Figures: 4; Supplemental Figures:10

Abstract

Almost four decades of research suggest a dynamic role of ductal epithelial cells in adipocyte adaptation in mammary gland white adipose tissue (mgWAT), but factors that mediate such communication are not known. Here, we identify a complex intercellular crosstalk in mgWAT revealed by single-cell RNA-seq (scRNA-seq) and comprehensive data analysis suggest that epithelial luminal cells during cold exposure undergo major transcriptomic changes that lead to the expression of an array of genes that encode for secreted factors involved in adipose metabolism such as Adropin (Enho), neuregulin 4 (Nrg4), angiopoietin-like 4 (Angptl4), lipocalin 2 (Lcn2), milk fat globule-EGF factor 8 (Mfge8), Insulin-like growth factor-binding protein 1 (Igfbp1), and haptoglobin (Hp). To define the mammary epithelial secretome, we coin the phrase "mammokines". We validated our cluster annotations and cluster-specific transcriptomics using eight different adipose scRNA-seq datasets including *Tabula Muris* and *Tabula Muris Senis*. In situ mRNA hybridization and ex vivo isolated mgWAT luminal cells show highly localized expression of mammokines in mammary ducts. Trajectory inference demonstrates that cold-exposed luminal cells have similar transcriptional profiles to lactation post-involution (PI), a phase defined by reappearance and maintenance of adipocytes in the mammary gland. Concomitantly, we found that under cold exposure female mgWAT maintains more adipogenic and less thermogenic potential than male scWAT. Conditioned media from isolated mammary epithelial cells treated with isoproterenol suppressed thermogenesis in differentiated beige/brown adipocytes and treatment of beige/brown differentiated adipocyte with LCN2 suppresses thermogenesis and increases adipogenesis. Finally, we find that mice lacking LCN2 show markedly higher cold-dependent thermogenesis in mgWAT than controls, and reconstitution of LCN2 in the mgWAT of

LCN2 knockout mice promotes inhibition of thermogenesis. These results show a previously unknown role of mammary epithelium in adipocyte metabolism and suggest a potentially redundant evolutionary role of mammokines in maintaining mgWAT adiposity during cold exposure. Our data highlight mammary gland epithelium as a highly active metabolic cell type and mammokines could have broader implications in mammary gland physiology and lipid metabolism.

Main

Adipose tissue is highly innervated with sympathetic nervous system (SNS) nerve fibers and activation of SNS by cold stress is known to induce lipolysis, fatty acid oxidation, and adipose thermogenesis by the expression of mitochondrial protein UCP1 which uncouples mitochondrial respiration to produce heat [1,2]. Much of the biology on the browning/beiging of WAT (white adipose tissue) has focused on the male posterior scWAT (subcutaneous white adipose tissue) depot that consists of dorsolumbar and inguinal WAT, which in female mice corresponds to mgWAT (mammary gland white adipose tissue).

Mammary glands are highly heterogenous tissue consisting of adipocytes and a stromal fraction composed of preadipocytes, mesenchymal stem cells, immune cells, endothelial cells, nerve fibers, and mammary ductal cells. The ductal cells are divided into myoepithelial cells, luminal hormone sensing, and luminal alveolar cells [3]. Mammary glands develop postnatally and ducts transition from a rudimentary phase to elaborate branching through inherent changes in luminal, basal, and alveolar cells. In virgin female mice, the mammary gland already has rudimentary ductal structures in the anterior and posterior scWAT and metabolic cooperativity between ductal cells and stroma is known to be important for mammary gland function and

development[3,4]. The profound changes in mammary ducts and adipocytes are seen during gestation, pregnancy, lactation, and post-involution [5,6]. The importance of adipocytes for mammary duct morphogenesis, and the dedifferentiation of adipocytes during lactation and reappearance during lactation post-involution, all suggest and a dynamic homeostatic interplay between ductal epithelial cells and adipocytes[6-8].

Result and Discussion

Comprehensive deconstruction of adrenergic induced changes in mgWAT by scRNA-seq

Compared to male mice, we noticed a highly variable and markedly less propensity of female mgWAT to beige under 24h cold exposure. We also noticed that 24 h cold-exposed male mice scWATs show a decrease in genes involved in adipogenesis and de novo lipogenesis such as Pparg, Lep, and Srebf1, whereas cold-exposed female mice mgWAT maintain the level of expression of those genes (Extended Data Fig. 1A). These data point toward a possible unique mechanism of mgWAT under cold stress to preserve adiposity[9]. For mechanistic insight into this phenomenon and to study cellular heterogeneity, inter-tissue communication, and cellular transcription dynamics in mgWAT in a thermogenic condition, we isolated stromal vascular fraction (SVF) from the mgWAT of 10 week old virgin female mice exposed to 24 cold or room temperature (RT) and performed single-cell RNA sequencing (scRNA-seq) (Fig. 1A). We obtained 12,222 of cells and used Cell Ranger software from 10X Genomics for data processing and the R package Seurat[10] to generate cell clusters and resolve their identities as previously described [11] (see Methods). We integrated our data set with eight other publicly available single cell data sets, from both SVF and mammary gland tissues including *Tabula Muris* and *Tabula Muris Senis* (Fig. 1B and Table 1) [12-15] for i) cell type validation, ii) to increase confidence in projected cell type, iii) sex and age

differences, and iv) mammary gland development (Fig. 1B). This integrated data set allowed us to precisely annotate various cell types present in mgWAT of female mice. Further subclustering analysis based on known cell type marker genes from our integrated approach identified clusters of a) adipocyte precursor cells (APCs), b) B cells, c) macrophages, d) T cells, e) endothelial cells, f) immune precursor cells (IPC), g) dendritic cells (DC) , h) Schwann cells, i) myoepithelial cells (myoep), and j) luminal-hormone sensing (Luminal-HS), luminal-alveolar (Luminal -AV), luminal-HS-AV, and myoepithelial cells (Fig. 1C and 1D).

To gain insight into the remodeling of stromal cells under adrenergic stress, we segregated the cumulative tSNE-plot into RT and COLD treatment by animal replicate (Fig. 1E). The tSNE and dot plots reveal global changes in relative proportions of SVF clusters between RT and cold (Fig. 1E and 1F). Among all the clusters APCs, macrophages, and luminal cells showed marked differences in cell type percentages (Fig. 1F) and appeared to have large differences in their global transcriptomic profiles in the t-SNE two-dimensional projection where cells from RT and cold were segregated (Fig. 1E). To quantitatively determine the transcriptional impact of cold treatment on individual cell types, we plotted fold change and adjusted p-values as a function of cluster types and found a high degree of transcriptional variation in APCs, macrophages, and luminal HS and AV under cold conditions (Fig. 1G). For the most varied cell types (APC, macrophage, and luminal cells), we subclustered these cell types and found two subclusters of APCs (APC1 and APC2) [16], four sub clusters of epithelial cells (myoepithelial, luminal HS, luminal AV, and luminal HS-AV), and 5 subclusters of myeloid cells (DNase 1l3+ macrophage, Fn+ macrophage, CD14+ macrophage, Retlng+ macrophage, and non-classical (Nc) macrophage) (Fig. 1H and 1I and Extended Data Fig. 1B, 1G, and 1H). The tSNE plots highlighted global transcriptional differences between RT and cold in subclusters (Extended Data Fig. 1B and 1H) and highly expressed genes

in those subclusters (Extended Data Fig. 1C and 1I). We then analyzed differentially expressed genes (DEGs) in APC, luminal, and macrophage clusters which were represented as a volcano plot with the ratio of fold change between cold and RT as a function of adjusted p-value. APCs showed an increase in expression of adipogenic genes such as *Cebpd* and *Klf9* [17-20] and a decrease in genes encoding for collagens suggesting and supporting the previous observation of adipogenesis under cold exposure (Extended Data Fig. 1D and 1E) [16]. Macrophages on the other hand namely CD14 macrophages and FN1 macrophages showed marked reduction in relative cell fraction and volcano plots demonstrated a decrease in *Tlr2*, *Rel* and *Nfkb* singling in Fn1 macrophages and increase in the expression of *Apoe2, Plin2 and Ddit4* in Cd14 and Fn1 macrophage (Extended Data Fig. 1J and 1K).

Identification of mammokines in mgWAT

Luminal cells showed a remarkable transcriptional difference in cell clusters between RT and cold, implicating a potential remodeling of the luminal epithelium upon cold exposure (Fig. 1G-1I). To gain insight into the crosstalk between cell types within the mgWAT SVFs at RT and cold, we applied a bioinformatics analysis, CellPhoneDB[21], an established method for inferring cell-cell communication from single cell RNA-seq. CellPhoneDB leverages a vast repository of curated receptors, ligands and their interactions to infer cell-cell communication. We focused our analysis on the communication between APCs and previously reported 24h cold-exposed mgWAT mature adipocytes single nuclei RNA-seq data (SNAP-seq) [22] with luminal epithelial cells within mgWAT (Extended Data Fig. 2). We noticed a prominent crosstalk between APCs and luminal cells via Wnt, Tgf, Tnf, BMPs, Ephrin signaling. Even though overall transcriptomic dynamics of luminal cells were increased, however, comparing with RT, cold stressed mice showed an overall decrease in the communication between the APCs and luminal cells (Extended Data Fig. 2). To

probe for cold-induced ligand-receptor interaction between APCs and luminal cells, we then focused our CellPhoneDB analysis on these cell types and found increases in NRGs, Wnt7B, BDNF and FGF1 signaling. These data indicate that under cold temperature luminal cells could elicit adipogenic signals to APCs by factors such as FGF1 and Wnts (Extended Data Fig. 2B) that could lead to an increase in adipogenic transcription factors such as CEBPD and KLF9 [23]. To test crosstalk between mature adipocytes and luminal cells, we analyzed the data reported in this study as a function of our published SNAP-seq [22] data, which is the first reported single nuclei RNA-seq data for adipocytes in mgWAT in females. Based on our analysis, we find that luminal cells have a distinct ligand-receptor interaction with mature adipocytes which are distinct to those observed in APCs (Extended Data Fig. 2C and 2D). We had previously reported 14 adipocyte subclusters in mgWAT [22] and among them we identified Cluster 12/14 as hormonally active adipocyte cluster, cluster 4 and 6 as traditional lipid storing adipocyte clusters, and cluster 9 as thermogenic adipocyte cluster. Our integrated CellPhoneDB data now show cold-induced signaling between luminal cells and i) Cluster 12/14 cells via receptor KIT ligand (KITLG) [24,25], ii) Cluster 4 and 6 via Wnt4 [26], and iii) cluster 9 by inhibitin beta B (Inhbb) [27] (Extended Data Fig. 2C and 2D)**.** Adipocyte are important for ductal morphogenesis and development [7] and our Cellphone DB data point toward a coordinated efforts of different kinds of mgWAT adipocytes in inducing luminal epithelium development. Besides these ligands, we also find an increase in VEGF, TGF, NOTCH, AREG, and, NECTIN4 signaling between adipocytes and luminal cells.

To probe if the ligands implicated in the CellPhoneDB analysis and other factors that are differentially expressed in luminal cells under cold exposure, we performed DEG analysis on RT and cold exposed luminal-HS/AV/HS-AV cells. We identified that several cold-induced genes from our CellPhoneDB analysis and upregulation of *Wnt4*, Adropin (*Enho*), leucine rich alpha-2

glycoprotein (*Lrg1*), Diglyceride acyltransferase (*Dgat2*), haptoglobin (*H*p), and angiopoietin-like 4 (Angptl4) in Luminal HS cells, lipocalin-2 (*Lcn2*), *Angptl4*, and Apolipoprotein B editing complex (*Apobec3*) in Luminal AV cells, and *Lrg1*, neuregulin 4 (*Nrg4*), ceruloplasmin (*Cp*), Angptl4 in Luminal HS-AV cells. Many of these gene encode for secreted factor that play important roles in lipid metabolism such as, ADROPIN, ANGPTL4, CP, NRG4, LCN2, and HP [28-37] (Fig. 1J). Overall, our combinatorial analysis demonstrate that mammary luminal cells have a diverse and complex secretome profile that could serves as a conduit for autocrine and paracrine signaling to potentially maintain metabolic homeostasis in the mgWAT and mammary gland morphogenesis. Together, we have termed the secretome of mammary luminal epithelial cells as "mammokines".

Some of the mammokines are known to be expressed by other cell types; however, we find that cold-induced mammokines and cold-induced luminal epithelial genes (ci-LEG) have distinct expression pattern and are highly enriched in EPCAM+ve epithelial cluster of mgWAT. Furthermore, Adrb2 and Adrb1 expression in luminal cells, suggest that these cells may directly respond to cold-induced SNS activation [38-40] (Fig. 1K). We next assessed the expression of mammokines and ci-LEG across different adipose depots in young and aged male and female mice. We queried the expression profiles of mammokines and ci-LEG in the *Tabula Muris* and *Tabula Senis* data set that include scRNA-seq from the SVFs of gonadal adipose tissue-GAT, mesenteric adipose tissue-MAT, and subcutaneous adipose tissue-SCAT, and mgWAT. The *Tabula Muris* scRNA-seq annotations from mgWAT showed five distinct cell clusters that include basal myoepithelial cells, two epithelial cells (HS and AV), endothelial cells , and stromal cells. (Extended Data Fig. 3A). Mammokines and ci-LEG showed mostly luminal epithelial cells enrichment and their expression did not vastly differ across various ages (Extended Data Fig. 3A-

3C). SVF scRNA-seq from GAT, MAT, SCAT from males and female mice showed specificity of mammokines and ci-LEG expression in female SCAT. However, genes such as Angptl4, Glul, and F3 were also expressed in APCs, endothelial cells, and myeloid cell populations (Extended Data Fig. 3D-3I). t-SNE plots of normalized gene expression levels for cold-induced mammokines in mgWAT (our study), male scWAT SVFs and mature adipocytes [22] show that Angptl4 and PRLR are also expressed by most mature adipocytes; however, other cold-induced mammokine genes showed relatively localized expression in luminal epithelial cells (Extended Data Fig. 3J)

Finally, to infer cold-induced transcription factor gene regulatory networks across all our scRNA-seq data sets we used SCENIC[41] (single-cell regulatory network inference and clustering) analysis to derive top 5 transcription factors enriched for the transcriptional state of each cell type. SCENIC revealed highly dynamic cold-induced transcription factor activity across all cell types and we found increased activity of COX14, IRX2, ELF5 ZFP708B, and TfFAP2A in luminal AV cells and FOXA1, BHLHE41, TEAD2, TFAP2B, and GRHL1 in Luminal HS cells (Fig. 1L and Extended data 4A-4C). Regulon activity implicated BHLHE41 as a master regulator of genes in luminal HS cells, and ELF5 showed a cold-specific gene transcriptional activity and could be directly involved in the expression of mammokines and ci-LEG such as *Lcn2* and *Igfbp5* (Extended Data Fig. 4D). ELF5 [42] is an important transcriptional regulator of mammary epithelial development and our data indicate ELF5 as an adrenergic-activated master regulator in luminal cells that could enhance expression of mammokines under cold stress.

Cold-induced mgWAT luminal cells resemble lactation post-involution transcriptomic state

In agreement with the data in Extended Fig. 3, our RNAscope fluorescent in situ hybridization (FISH) analysis showed a highly localized expression of mammokines *Enho, Lrg1, Lcn2, Hp,*

Nrg4, and *Wnt4* in Epcam+ve mammary ductal cells (Fig. 2A and Extended Data Fig. 5). To probe for a possible role of cold induced mammokines and ci-LEG in mgWAT physiology, we next performed trajectory inference using Slingshot [43] from mammary gland EPCAM+ve cells at nulliparous (NP), gestation (G), lactation (L), and lactation post-involution (PI) [12] (Fig. 2B) . Our analysis showed distinct nodal points for different mgWAT states (NP, G, L, and PI) and co-clustering of RT and cold luminal HS, AV, and HS-AV cells (Fig. 2C and 2D, Extended Data Fig. 6 and 7). RT and cold luminal HS, AV, and HS-AV demonstrated a distinct co-clustering with various stages of mgWAT development (Extended Data Fig 6-9). Luminal-AV under RT condition showed transcriptomic enrichment with G phase and luminal-HS in RT condition showed a shared enrichment in G, PI, and NP phase, whereas luminal-HS-AV under in RT showed enrichment in both NP and PI phase (Extended Data 8 and 9). Cold exposed luminal AV, luminal HS, and luminal HS-AV showed a markedly high and specific co-clustering with cells in the PI phase of the mammary gland. Cold-induced mammokines such as Mfge8 [44], Igfbp5, Lrg1, Angptl4 [28], Hp, and Lcn2 were mostly abundant in the luminal AV, HS-AV, and PI (Fig. 2C-2F, Extended Data 6B and 6C and 7B and 7C). PI is a stage in the mammary gland where adipocytes reappear and fill the fat pad [8]. Taken together, our CellPhoneDB analysis, SCENIC, DEG analysis, and trajectory inference suggest that mgWAT luminal cells of female mice during cold-exposure could produce mammokines that may act to promote adiposity in mgWAT by facilitating adipogenesis and adipocyte expansion, and blockade of thermogenesis. Our integrated analyses further supports the data in Extended Data Fig. 1A, where we report a markedly less propensity of females mgWAT to beige and higher capacity of mgWAT to maintain adiposity following cold exposure.

Cold-induced mammokines inhibit adrenergic-dependent adipose thermogenesis

To experimentally validate our analysis and increase in EPCAM+ve luminal cell population (Fig. 3A), we first purified EPCAM+ve and EPCAM-ve cells from mgWAT of RT and cold-exposed mice and then stained for EPCAM and CD49F for FACS analysis. As shown in Fig. 3B, we saw three distinct populations of cells that were $EPCAM^{lo}CD49F^{lo}$ (stromal), $EPCAM^{hi}$ $CD49F^{hi}$(luminal), and $EPCAM^{+ve}CD49F^{hi}$ (basal) cells. Luminal cells were only enriched in EPCAM+ve purified cells and showed a significant cold-dependent increase in cell population compared to RT condition, in agreement with our scRNA-seq data. We also noticed a marked reduction in the basal cell population upon cold treatment in EPCAM+ve selected cells, indicating a differential response to cold stress by luminal and basal cell in ducal epithelium. To test whether luminal cells directly responded to cold-induced SNS activation, we tested mammokine expression on isolated primary mgWAT EPCAM+ve and EPCAM-ve cells from RT or cold mice or cultured primary mgWAT EPCAM+ve and EPCAM-ve cells that were either treated or not treated with isoproterenol. Cold-induced mammokines were highly enriched in EPCAM+ve cells and showed increased expression upon isoproterenol or cold treatment (Fig 3C-3E). To test if adrenergic-dependent secretion from mammary epithelial cells blocked adipocyte thermogenesis, we treated normal mammary epithelial cell NMuMG with varying concentration of isoproterenol and then treated brown/beige differentiated 10T1/2 cells with the conditioned media from NMuMG cells. Consistent with the data in Fig. 3D, we find a dose-dependent increase in cold-induced mammokines and reciprocal decrease in thermogenic genes in conditioned media treated beige/brown differentiated 10T1/2 cells (Fig. 3F and 3G). We further directly tested the roles of mammokines LRG1 and LCN2 by treating beige differentiated preadipocytes with recombinant LRG1 or LCN2. As shown in Fig 3H and 3I, LRG1 and LCN2 caused a significant reduction in thermogenic gene expression.

LCN2 is a mammokine involved in maintaining mgWAT adiposity

Overall, our broad scRNA-seq data and targeted experimental data consistently identify LCN2 as a mammokine that is i) highly enriched in mammary luminal epithelial cells, ii) induced by both cold and isoproterenol treatment, iii) expressed mostly in the PI phase of mammary gland, iv) and potentially regulated by the activity of ELF5 in luminal cells under cold stress. The secretion of LCN2 by luminal AV and HS-AV cells could potentially be a mechanism of luminal cells to block excess lipid mobilization, thermogenesis, and preserve adiposity. Consistent with data in Fig.1 and Fig. 3, both isoproterenol treatment and cold exposure led to an increase in Lcn2 levels in EPCAM+ve mammary ducts (Fig. 4A). To test the physiological role of LCN2 in regulating mgWAT adiposity, we mimicked cold induction of LCN2 in mgWAT by inducing LCN2 exogenous expression specifically in mgWAT of LCN2KO mice by injecting adipoAAV-LCN2 or adipoAAV-GFP [31] (See Methods). Our unbiased bulk RNA-seq data show that LCN2 expression was not supraphysiological compared to controls and the volcano plot in Fig. 4B showed that LCN2 exogenous expression causes a significant decrease in thermogenic genes such as *Ucp1, Cidea, Ppara* and increase in adipogenic genes such *as Lep, Mmp12* [45,46], *Zfp423* [47], and Lbp [48]. LCN2 expression also led to an increase in *Aldh1a1,* which was recently shown to inhibit adipose thermogenesis by downregulating UCP1 levels [49,50]. We validated our RNA-seq data by directed qPCR in both LCN2 reconstituted mgWAT of LCN2KO and WT mice (Fig. 4C). Finally, to test the role of LCN2 under cold stress, we exposed female LCN2KO and WT mice to 24 h cold exposure. LCN2KO mice mgWAT showed more beiging/browning and gene expression analysis showed a significant increase in thermogenic genes such as Ucp1 and decreases in adipogenic genes such as Lep indicating that LCN2 is potentially one of the limiting factors involved in

regulating the propensity of mgWAT to beige (Fig. 4D and 4E). However, paradoxically, we noticed that cold exposed LCN2KO mice mgWAT showed increase in de novo lipogenic genes, which could suggest a potential negative feedback loop to compensate excess for lipid mobilization [51]. Compared to males, LCN2KO females had significantly decreased in body and mgWAT weight (Extended Fig. 10A and 10B). We noticed both sexes had an increase in plasma free glycerol and decrease in free fatty acid (FFA), implicating a potential local effect of mammokines on the local interaction between epithelium and adipocyte metabolism. However, plasma triglyceride levels were significantly lower in male LCN2KO compared to controls whereas TG levels were comparable between LCN2KO and WT mice (Extended Data Fig. 10C-10E). Overall, our scRNA-seq analysis and both our tissue-specific gain-of-function and loss-of-function experimental data show LCN2 as a factor expressed in luminal cells that function to maintain adiposity in mgWAT during cold-stress.

Figure Legends

Figure 1. Deconstruction of mgWAT shows cold-induced remodeling of mammary epithelium

(A) Cartoon depiction of the scRNA-seq workflow showing isolation of stromal vascular fraction (stromal cells) from mammary fat pad (mgWAT) of 10 week old 24 h RT or COLD exposed female mice.

(B) UMAP plots of integrated single cell data from this study and 8 external datasets (see Methods). Each point represents a single cell which are colored by dataset (left panel) and cell type (right panel).

(C) Expression of known canonical markers for cell types in the SVF and mammary gland. Color corresponds to average expression level and size corresponds to percentage of cells which express the gene.

(D) t-SNE plot of single cells from mammary gland and surrounding SVF colored by cell type. Cell types were identified based on expression of canonical marker genes.

(E) t-SNE plot of single cells from mammary gland and surrounding SVF colored by cell type and separated by sample. Relative fraction of each cell type in each sample is indicated on each cluster. Room temperature samples are on the top row and 4-degree samples are on the bottom row.

(F) Relative fractions of cell types within each sample. Black dot indicates the average relative fractions across all samples.

(G) Differentially expressed genes between 4 degree treated mice and RT animals across all cell types. Significant DEGs (adjusted p-value < 0.05) are highlighted with the average log fold change between 4 degree and RT indicated on the y-axis.

(H) UMAP plot of subclustering of luminal single cells colored by cell type. Luminal-HS: blue, Luminal-HS-AV: red, and Luminal-AV: yellow.

(I) UMAP plot of subclustering of luminal single cells color by condition. Room temperature treated animals: red and 4-degree treated animals: blue.

(J) Volcano plots of differentially expressed genes in luminal cells between 4-degree treated animals and room temperature animals.

(K) UMAP plots of normalized gene expression levels for genes of interest in luminal cells.

(L) Heatmap of normalized transcription factor regulon specificity (columns) for APCs, luminal cells, and Cd14 macrophages (rows) derived using SCENIC for single cells from animals at room

temperature (left) and at 4 degrees (right). The top five transcription factor regulons for each luminal cell type were identified using SCENIC in animals at room temperature (top) and at 4 degrees (bottom).

Abbreviations: APC, adipose precursor cells; IPC, immune precursor cells; Mac, macrophages; ncMon, non-classical monocytes; cDC, conventional dendritic cells; migDC, migratory dendritic cells; pDC, plasmacytoid dendritic cells; Tregs, regulatory T cells; mCd4T, memory Cd4 T cells; nCd4T, naïve Cd4 T cells; aCd8T, activated Cd8 T cells; Myoep, myoepithelial cells; VEndo, vascular endothelial cells; Endo-Tip, endothelial tip cells; Endo-Stalk, endothelial stalk cells; Lymph, lymphatic endothelial cells; Peri, pericytes; Luminal-HS, hormone-sensing luminal cells; Luminal-AV, secretory alveolar luminal cells; Luminal-HS-AV.

Figure 2. Cold-induced mammokines are enriched in mammary ducts at the lactation PI transcriptional state.

A) RNAScope FISH (see Materials and methods) of indicated probes from mgWAT of 24h cold exposed mice.

(B) UMAP plot of subclustering of differentiation of mammary epithelial cells colored by cell type.

(C) Trajectory inference of publicly available data on the differentiation of mammary epithelial cells integrated with the luminal alveolar cells data from this study using Slingshot. Cells are colored by cell type.

(D) Trajectory inference of publicly available data on the differentiation of mammary epithelial cells integrated with the hormone sensing luminal cells data from this study using Slingshot. Cells are colored by cell type.

(E) Normalized expression of genes of interest overlaid on the trajectory inference of luminal alveolar cells.

(F) Normalized expression of genes of interest overlaid on the trajectory inference of hormone sensing luminal cells.

Abbreviations: Hsp – hormone sensing progenitors; Hsd – hormone sensing differentiated; Lp – luminal progenitor; Avd – differentiated alveolar cells; Avp – progenitor alveolar cells; G – gestation; L – lactation; NP – nulliparous; PI – post-involution; RT – room temperature; 4DEG – 4 degrees.

Figure 3. Cold-induced mammokines inhibit adipose thermogenesis.

A) t-SNE plot showing normalized gene expression levels for EPCAM in luminal cells RT or Cold exposed mice.

B) Representative FACS plot of CD49f and Epcam expression in Epcam bead selected Epcam+ve or Epcam-ve epithelial cells from RT or cold mice. 2 mice per condition and 4 mammary fat pad per mice

C) Cartoon depiction of selecting and plating Epcam+ve cells from SVF of mgWAT

D) Real-time qPCR of indicated genes from primary mgWAT Epcam-ve (EPCAM-NEG) and Epcam+ve (EPCAM-Pos) cells treated with and without 10 µM isoproterenol (ISO) for 24h.

E) Real-time qPCR of indicated genes from RT or cold exposed mice primary mgWAT Epcam-ve (EPCAM-NEG) and Epcam+ve (EPCAM-Pos) cells.

F) Real-time qPCR of indicated genes for Nmumg cells treated with indicated concentrations of isoproterenol for 24h.

G) Real-time qPCR of indicated genes in D6 differentiated beige/brown 10T1/2 cells treated with conditioned media from (F)

H) Real-time qPCR of indicated genes in D8 differentiated beige/brown 10T1/2 cells treated with indicated concentration of recombinant LRG1 for 24h

I) Real-time qPCR of indicated genes in beige/brown D8 differentiated primary SVFs from mgWAT of LCNKO mice treated with indicated concentration of recombinant LRG1 for 24h

Figure 4. LCN2 preserves mgWAT adiposity.

A) RNAScope FISH (see Materials and methods) of indicated probes from mgWAT of RT or 24h isoproterenol or cold exposed mice.

B) Volcano of DEG from the mgWAT of LCN2KO mice treated with adipose-specific AAV-LCN2 or AAV-GFP and represented as a fold change of LCN2/GFP ratio as a function of p-value. Genes labelled are either induced (+) or repressed (-) by LCN2.

C) Real-time qPCR of indicated genes from the mgWATs of LCN2KO or WT mice treated with AAV-LCN2 or AAV-GFP.

D and E) Gross pathology (D) and real-time qPCR of indicated genes (E) of mgWAT from 24 cold exposed WT or LCN2KO mice.

Extended Data Figure Legends

Figure 1.

A) Real-time qPCR of indicated genes from female mgWAT or male scWAT exposed to RT or 24h cold.

B) UMAP plot of subclustering of adipose precursor cells colored by cell type. APC1 cells are colored red and APC2 cells are colored blue.

C) UMAP plots of normalized gene expression levels for canonical marker genes in adipose precursor cells.

(D) Volcano plots of differentially expressed genes in APC1 cells between 4-degree treated animals and room temperature animals.

(E) Volcano plots of differentially expressed genes in APC2 cells between 4-degree treated animals and room temperature animals.

(F) UMAP plots of normalized gene expression levels for indicated genes of interest in adipose precursor cells.

(G) UMAP plot of subclustering of myeloid cells colored by cell type cluster.

(H) UMAP plot of subclustering of myeloid cells colored by condition. Room temperature treated animals: red and 4-degree treated animals: blue.

(I) UMAP plots of normalized gene expression levels for genes of interest in myeloid cells.

(J) Volcano plots of differentially expressed genes in Cd14+ macrophages between 4-degree treated animals and room temperature animals.

(K) Volcano plots of differentially expressed genes in Fn1+ macrophages between 4-degree treated animals and room temperature animals.

(L) UMAP plots of normalized gene expression levels for canonical marker genes in myeloid cells.

Figure 2

(A) Mean expression and p-values of ligand-receptor interactions which were more prevalent at room temperature for all pairwise combinations of APCs and luminal cell types.

(B) Mean expression and p-values of ligand-receptor interactions which were more prevalent at 4 degrees for all pairwise combinations of APCs and luminal cell types.

(C) Mean expression and p-values of ligand-receptor interactions which were more prevalent at room temperature for all pairwise combinations of luminal cell types and mature adipocyte cell clusters.

(D) Mean expression and p-values of ligand-receptor interactions which were more prevalent at 4 degrees for all pairwise combinations of luminal cell types and mature adipocyte cell clusters.

Figure 3

(A) UMAP plot of subclustering of mammary gland cells from Tabula Senis using FACs and Smart-Seq2 colored by cell type.

(B) UMAP plots of normalized gene expression levels for genes of interest in mammary gland cells from Tabula Senis using FACs and Smart-Seq2.

(C) Violin plots of normalized gene expression levels for genes of interest in mammary gland cell types from Tabula Senis using FACs and Smart-Seq2, colored by age of mouse.

(D) UMAP plot of subclustering of stromal vascular fraction from Tabula Senis using 10X Genomics colored by cell type.

(E) UMAP plot of subclustering of stromal vascular fraction cells from Tabula Senis using 10X Genomics colored by mouse age.

(F) UMAP plots of normalized gene expression levels for indicated genes of interest in stromal vascular fraction cells from Tabula Senis using 10X Genomics.

G) UMAP plot of subclustering of stromal vascular fraction cells from Tabula Senis using 10X Genomics colored by sex.

(H) UMAP plot of subclustering of stromal vascular fraction cells from Tabula Senis using 10X Genomics colored by adipose depot.

(I) Violin plots of normalized gene expression levels for genes of interest in stromal vascular fraction cells from female mice from Tabula Senis using 10X Genomics, colored by age of adipose depot.

(J) UMAP plots of normalized gene expression levels for genes of interest across multiple datasets including: female mammary gland white adipose tissue and stromal vascular fraction, mammary gland data from Tabula Muris, mature adipocytes, and male subcutaneous what adipose tissue and stromal vascular fraction.

Abbreviations: Hsp – hormone sensing progenitors; Hsd – hormone sensing differentiated; Lp – luminal progenitor; Avd – differentiated alveolar cells; Avp – progenitor alveolar cells; Bsl – basal cells; Myo – myoepithelial cells; Prc – Procr+ cells; G – gestation; L – lactation; NP – nulliparous; PI – post-involution

Figure 4

(A) The top five transcription factor regulons for all cell types in the mammary gland (this study) and surrounding SVF at room temperature were identified using SCENIC.

(B) The top five transcription factor regulons for all cell types in the mammary gland (this study) and surrounding SVF at 4 degrees were identified using SCENIC.

(C) Heatmap of normalized transcription factor regulon specificity (columns) for all cell types in the mammary gland and surrounding SVF at room temperature (top) and 4 degrees (bottom) derived using SCENIC.

(D) Subnetworks of transcription factor regulons of interest for Bhlhe41 in hormone sensing luminal cells (Up) and Elf5 in luminal alveolar cells (Down) derived using SCENIC. Transcription factors indicated in diamonds in the center and genes in the regulon in the surrounding circles.

Genes in red were derived from the room temperature data, genes in blue were derived from the 4-degree data, and genes with both were present in the regulons in both conditions. Red arrow show cold-induced mammokines.

Figure 5

(A-E) RNAscope FISH for indicated probes from RT or cold exposed female mice mgWAT.

Figure 6

(A) UMAP plot of integrated publicly available data on the differentiation of mammary epithelial cells with the luminal alveolar cells from this study, colored by cell type (top panel). The fraction of each cell type in clusters defined by Louvain clustering is indicated by pie charts (bottom panel) with the color in the pie chart corresponding to the cell type color in the top panel.

(B) Violin plots of normalized gene expression levels for genes of interest in integrated publicly available data on the differentiation of mammary epithelial cells with the luminal alveolar cells from this study, colored by cell type.

(C) UMAP plots of normalized gene expression levels for genes of interest in integrated publicly available data on the differentiation of mammary epithelial cells with the luminal alveolar cells from this study.

Abbreviations: Lp – luminal progenitor; Avd – differentiated alveolar cells; Avp – progenitor alveolar cells; G – gestation; L – lactation; NP – nulliparous; PI – post-involution; RT – room temperature; 4DEG – 4 degrees.

Figure 7

(A) UMAP plot of integrated publicly available data on the differentiation of mammary epithelial cells with the hormone sensing luminal cells from this study, colored by cell type (top panel). The fraction of each cell type in clusters defined by Louvain clustering is indicated by pie charts (bottom panel) with the color in the pie chart corresponding to the cell type color in the top panel.

(B) Violin plots of normalized gene expression levels for genes of interest in integrated publicly available data on the differentiation of mammary epithelial cells with the hormone sensing luminal cells from this study, colored by cell type.

(C) UMAP plots of normalized gene expression levels for genes of interest in integrated publicly available data on the differentiation of mammary epithelial cells with the hormone sensing luminal cells from this study.

Figure 8

(A) Trajectory inference of publicly available data on the differentiation of mammary epithelial cells integrated with the luminal alveolar cells data from this study using Slingshot. Cells are colored by cell type. Normalized expression of genes specific to cluster #1 overlaid on the trajectory inference of luminal alveolar cells.

(B) Trajectory inference of publicly available data on the differentiation of mammary epithelial cells integrated with the luminal alveolar cells data from this study using Slingshot. Cells are colored by cell type. Normalized expression of genes specific to cluster #6 overlaid on the trajectory inference of luminal alveolar cells.

(C) Trajectory inference of publicly available data on the differentiation of mammary epithelial cells integrated with the luminal alveolar cells data from this study using Slingshot. Cells are colored by cell type. Normalized expression of genes specific to cluster #3 overlaid on the trajectory inference of luminal alveolar cells.

(D) Heatmap of genes which are specific to each cluster in the trajectory inference of publicly available data on the differentiation of mammary epithelial cells integrated with the luminal alveolar cells data from this study using Slingshot

Abbreviations: Hsp – hormone sensing progenitors; Hsd – hormone sensing differentiated; Lp – luminal progenitor; Avd – differentiated alveolar cells; Avp – progenitor alveolar cells; G – gestation; L – lactation; NP – nulliparous; PI – post-involution; RT – room temperature; 4DEG – 4 degrees.

Figure 9

(A) Trajectory inference of publicly available data on the differentiation of mammary epithelial cells integrated with the hormone sensing luminal cells data from this study using Slingshot. Cells are colored by cell type. Normalized expression of genes specific to cluster #3 overlaid on the trajectory inference of hormone sensing luminal cells.

(B) Trajectory inference of publicly available data on the differentiation of mammary epithelial cells integrated with the hormone sensing luminal cells data from this study using Slingshot. Cells are colored by cell type. Normalized expression of genes specific to cluster #4 overlaid on the trajectory inference of hormone sensing luminal cells.

(C) Trajectory inference of publicly available data on the differentiation of mammary epithelial cells integrated with the hormone sensing luminal cells data from this study using Slingshot. Cells

are colored by cell type. Normalized expression of genes specific to cluster #2 overlaid on the trajectory inference of hormone sensing luminal cells.

(D) Heatmap of genes which are specific to each cluster in the trajectory inference of publicly available data on the differentiation of mammary epithelial cells integrated with the hormone sensing luminal cells from this study using Slingshot

Abbreviations: Hsp – hormone sensing progenitors; Hsd – hormone sensing differentiated; Lp – luminal progenitor; G – gestation; L – lactation; NP – nulliparous; PI – post-involution; RT – room temperature; 4DEG – 4 degrees.

Abbreviations: Hsp – hormone sensing progenitors; Hsd – hormone sensing differentiated; Lp – luminal progenitor; G – gestation; L – lactation; NP – nulliparous; PI – post-involution; RT – room temperature; 4DEG – 4 degrees.

Figure 10

A) Body weight of LCN2KO or WT male and female mice.

B) Indicated fat pad weight of LCN2KO or WT male and female mice.

C-E) Plasma free glycerol, free fatty acid (FFA), and triglyceride (TG) levels from male and female at RT or 24 cold-exposed.

Methods

Animal Studies

C57BL/6 WT males and female mice (#000664) and LCN2KO (#24630) were acquired from Jackson Laboratory and maintained in a pathogen-free barrier-protected environment (12:12 h light/dark cycle, 22°C-24°C) at the UCLA and Mount Sinai animal facility. For the time course cold exposure experiment, WT mice at 8-10 weeks of age were singly housed at 4°C room in a

non-bedded cage without food and water for first 6 h; thereafter food, water, and one cotton square were added. For the 24 h harvest, 3 h before harvest, food, water, and cotton square were removed and then mice were harvested. At the end of the experiment, mgWATs were resected for analysis. For overexpression studies, recombinant adeno-associated virus serotype 8 (AAV8) expressing LCN2 or GFP was generated and injected as described previously [31]. Animal experiments were conducted in accordance with the Mount Sinai and UCLA Institutional Animal Care and Research Advisory Committee.

RNA-Seq

RNA isolation, library preparation, and analysis were conducted as previously described [31]. Flash-frozen mgWAT samples were homogenized in QIAzol (Qiagen, Germantown, MD), and following chloroform phase separation, RNA was isolated according to the manufacturer's protocol using miRNeasy columns (Qiagen, Germantown, MD). Libraries were prepared from extracted mgWAT fat RNA (Agilent 2200 Tapestation eRIN >8.2) using KAPA Stranded mRNA-Seq Kit (cat #KK8421, KAPA Biosystems, Wilmington, MA), per the manufacturers' instructions. The pooled libraries were sequenced with an Illumina HiSeq4000 instrument, SE50bp reads (Illumina, San Diego, CA). Reads were aligned to the mouse genome mm10 using STAR [52] or HISAT2[53] aligner and quantified using the Bioconductor R packages as described in the RNA-Seq workflow [54]. *P* values were adjusted using the Benjamini-Hochberg procedure of multiple hypothesis testing[54].

Single cell isolation from SVF

Single cell SVF populations from adipose tissue were isolated as described previously[22,55]. The fourth inguinal white adipose tissue (iWAT) depot mgWAT from mice exposed to cold stress (4°C) or room temperature for 24 hr was dissected and placed on a sterile 6-well tissue culture plate with ice-cold 1X DPBS. Excess liquid was removed from fat pads by blotting. Each tissue was cut and minced with scissors and then placed in 15 ml conical tubes containing digestion buffer (2 ml DPBS and Collagenase II at 3 mg/ml; Worthington Biochemical, Lakewood, NJ, USA) for 40 min of incubation at 37°C with gentle shaking at 100 rpm. Following tissue digestion, enzyme activity was stopped with 8 ml of resuspension media (DMEM/F12 with glutamax supplemented with 15%FBS and 1% pen/strep; Thermo Scientific, CA). The digestion mixture was passed through 100 µm cell strainer and centrifuged at 150 x g for 8 min at room temperature. To remove red blood cells, the pellet was resuspended and incubated in RBC lysis buffer (Thermo Scientific, CA) for 3 min at room temperature, followed by centrifugation at 150 x g for 8 min. The pellet was then resuspended in resuspension media and again spun down at 150 x g for 8 min. The cell pellet was resuspended in 1 ml of 0.01% BSA (in DPBS) and passed through a 40 µm cell strainer (Fisher Scientific, Hampton, NH, USA) to discard debris. Cell number was counted for 10X Genomics single cell application.

SVF single cell barcoding and library preparation

To yield an expected recovery of 4000-7000 single cells, an estimated 10,000 single cells per channel were loaded onto Single Cell 3' Chip (10X Genomics, CA). The Single Cell 3' Chip was placed on a 10X Genomics instrument to generate single cell gel beads in emulsion (GEMs). Chromium Single Cell 3' v3 Library and Cell Bead Kits were used according to the manufacturer's instructions to prepare single cell RNA-Seq libraries.

Illumina high-throughput sequencing libraries

Qubit Fluorometric Quantitation (ThermoFisher, Canoga Park, CA, USA) was used to quantify the 10X Genomics library molar and a TapeStation (Aligent, Santa Clara, CA, USA) was used to estimated library fragment length. Libraires were pooled and sequenced on an Illumina HiSeq 4000 (Illumina, San Diego, CA, USA) with PE100 reads and an 8 bp index read for multiplexing. Read 1 contained the cell barcode and UMI and read 2 contained the single cell transcripts.

Single cell data pre-processing and quality control

To obtain digital gene expression matrices (DGEs) in sparse matrix representation, paired end reads from the Illumina HiSeq 4000 were processed and mapped to the mm10 mouse genome using 10X Genomics' Cell Ranger v3.0.2 software suite. Briefly, .bcl files from the UCLA Broad Stem Cell Research Center sequencing core were demultiplexed and converted to fastq format using the 'mkfastq' function from Cell Ranger. Next, the Cell Ranger 'counts' function mapped reads from fastq files to the mm10 reference genome and tagged mapped reads as either exonic, intronic, or intergenic. Only reads which aligned to exonic regions were used in the resulting DGEs.

After combining all four sample DGEs into a single study DGE, we filtered out cells with (1) UMI counts < 700 or > 30,000, (2) gene counts < 200 or > 8,000, and (3) mitochondrial gene ratio > 10%. This filtering resulted in a dataset consisting of 42,052 genes across 12,222 cells, with approximately 2,300 – 4,650 cells from each sample. A median of 2,411 genes and 7,252 transcripts were detected per cell.

Identification of cell clusters

To achieve high resolution cell type identification and increased confidence in our cell type clustering we brought in external publicly available single cell data from SVF and mammary tissues. Specifically, we included single cell data from 9 datasets comprising 91,577 single cells from the mammary gland and multiple adipose depots, across 4 different single cell platforms (**Table 1**). These external datasets and the SVF data from this study were all independently normalized using sctransform[56] and integrated using Seurat[57,58] v3.1.5. The single cell expression profiles were projected into two dimensions using UMAP[59] or tSNE[60] and the Louvain[61] method for community detection was used to assign clusters. This integrated data was only used to identify and define the cell types. All plots which are not explicitly designated as integrated with at least one external dataset and all downstream analyses (e.g. differential expression analyses) were conducted on non-integrated data to retain the biological effect of the cold treatment. Visualization of the non-integrated data was conducted on a subsampled dataset where all samples had the same number of cells to give an equal weight to each sample, however, all downstream analyses (e.g. differential expression analyses) leveraged the full dataset.

Cell #	Tissue	Sex	Condition	Technology	Name	Source
22,800	BAT, EPI, ING)	M	SVF	Drop-Seq	Broad SVF	Broad Single Cell Portal[62]
25,010	Mammary	F	NP, G, L, PI	10X Genomics	MammaryEpi	GSE106273[63]
14,927	Mammary	F	NP, G, L, PI	Microwell-seq	MouseCellAtlas	figshare[64,65]
4,481	Mammary	F	N/A	10X Genomics	TM.Mammary.10X	figshare[13,66]
2,405	Mammary	F	N/A	FACS + Smart-seq2	TM.Mammary.FACS	figshare[13,66]
4,967	SVF (BAT, GAT,	F, M	N/A	FACS + Smart-seq2	TM.SVF.FACS	figshare[13,66]

	MAT, SCAT)					
3,132	Mammary	F	Age (3m, 18m, 21m)	FACS + Smart-seq2	TS.Mammary.FACS	figshare[14,67]
5,080	SVF (BAT, GAT, MAT, SCAT)	F, M	Age (18m, 21m, 30m)	10X Genomics	TS.SVF.10X	figshare[14,67]
8,775	SVF (BAT, GAT, MAT, SCAT)	F, M	Age (3m, 18m, 24m)	FACS + Smart-seq2	TS.SVF.FACS	figshare[14,67]

Table 1: Publicly available single cell datasets used in this study

BAT – brown adipose tissue, EPI – epididymal white adipose tissue, ING – inguinal white adipose tissue, NP - nulliparous, G - gestation, L – lactation, PI - post involution, GAT – gonadal adipose tissue, MAT – mesenteric adipose tissue, SCAT – subcutaneous adipose tissue

Cell type-specific gene expression signatures

Cell type-specific gene expression signatures were generated by identifying genes with expression levels two-fold greater (adjusted p-values < 0.05) than all other cell types. To ensure consistency across samples, Seurat's FindConservedMarkers function (Wilcoxon rank sum test with a meta p-value) was applied across each sample.

Resolving cell identities of the cell clusters

To identify the cell type identity of each cluster, we used a curated set of canonical marker genes derived from the literature (**Supplementary Table 1**) to find distinct expression patterns in the cell clusters. Clusters which uniquely expressed known marker genes were used as evidence to

identify that cell type. Cell subtypes which did not express previously established markers were identified by general cell type markers and novel markers obtained with Seurat's FindConservedMarkers function were used to define the cell subtype.

Quantitative assessment of global transcriptome shifts

Quantitative assessment of global transcriptome shifts in each cell type due to cold treatment was assessed using a previously established Euclidean distance-based approach[11]. Briefly, average gene expression profiles for each condition (room temperature and cold treated) were generated for each cell type. After representing the gene expression as a z-score and only considering the top 1000 most highly expressed genes in each cell type, the Euclidean distance between room temperature and cold treated conditions was calculated for each cell type. To assign significance to the distances, a null distribution was estimated by calculating the Euclidean distance between two groups of randomly sampled cells of the given cell type. This permutation approach was repeated 1000 times and compared to the Euclidean distance from the true group labels to determine an empirical p-value. This p-value was adjusted for multiple testing with a Bonferroni correction.

Differential gene expression analysis

Within each identified cell type, cold treated and room temperature single cells were compared for differential gene expression using Seurat's FindMarkers function (Wilcoxon rank sum test) in a manner similar to Li et al.[15]. Differentially expressed genes were identified using two criteria: (i) an expression difference of >= 1.5 fold and adjusted p-value < 0.05 in a grouped analysis between room temperature mice (n = 2) and cold treated mice (n = 2); (ii) an expression difference of >=

1.25 fold and consistent fold change direction in all 4 possible pairwise combinations of cold-treated vs room temperature mice.

Pathway enrichment analysis

Pathway enrichment analysis was conducted on the differentially expressed genes from each cell type using gene sets from KEGG[68], Reactome[69], BIOCARTA[70], GO Molecular Functions[71], and GO Biological Processes[71]. Prior to enrichment, mouse gene names were converted to human orthologues. Enrichment of pathways was assessed with a Fisher's exact test, followed by multiple testing correction with the Benjamini-Hochberg method. Gene set enrichments with FDR < 0.05 were considered statistically significant.

CellPhoneDB analysis

To predict cell-cell interactions with the single cell data, we used the CellPhoneDB method[21]. Breifly, CellPhoneDB has a curated database of >2400 interactions in the categories of protein-protein interactions, secreted and membrane proteins, and protein complexes. This database was used to identify enriched receptor-ligand interactions between two cell types based on the expression of a receptor by one cell type and the corresponding ligand by another cell type. Significance was obtained using a permutation approach. We applied CellPhoneDB to each sample separately and only considered interactions between cell types significant if it was observed in both samples a particular group (e.g. room temperature or cold treated). Since the curated database of interactions is based on human genes, we first converted our mouse genes to their human orthologues.

Lineage trajectory inference

Prior to lineage trajectory inference, the SVF single cell data from this study was integrated with a dataset demonstrating the differentiation dynamics of mammary epithelial cells[7] using Seurat as described in the "Identification of cell clusters" section. Lineage trajectory inference was performed on this integrated dataset by applying slingshot[43] which was wrapped in a docker container as part of the dynverse[72].

Gene regulatory network inference

Gene regulatory network inference was performed with pySCENIC[41] following the workflow described by Van de Sande et al[73]. Briefly, starting with counts data, gene modules which are co-expressed with transcription factors were identified with GRNBoost2[74]. Next, candidate regulons were created from transcription factor – target gene interactions and indirect targets were pruned based on motif discovery with cisTarget[41]. Finally, regulon activity was quantified at cellular resolution with AUCell[41] which allowed for the prioritization of regulons for each cell type based on the quantified activity.

Real time qPCR

Total RNA was isolated using TRIzol reagent (Invitrogen) and reverse transcribed with the iScript cDNA synthesis kit (Biorad). cDNA was quantified by real-time PCR using SYBR Green Master Mix (Diagenode) on a QuantStudio 6 instrument (Themo Scientific, CA). Gene expression levels were determined by using a standard curve. Each gene was normalized to the housekeeping gene 36B4 and was analyzed in duplicate. Primers used for real-time PCR are available upon request.

RNAScope Fluorescence in situ hybridization (FISH)

mgWAT from RT or cold exposed mice (Jackson Laboratory, #000664) was fixed in 10% formalin overnight, embedded with paraffin, and sectioned into unstained, 5 µm-thick sections. Sections were baked at 60°C for 1 hour, deparaffinized, and baked again at 60°C for another hour prior to pre-treatment. The standard pre-treatment protocol was followed for all sectioned tissues. *In situ* hybridization was performed according to manufacturer's instructions using the RNAscope Multiplex Fluorescent Reagent Kit v2 (#323136, Advanced Cell Diagnostics [ACD], Newark, CA). Opal fluorophore reagent packs (Akoya Biosciences, Menlo Park, CA) for Opal 520 (FP1487A), Opal 570 (FP1488A), and Opal 620 (FP1495A), and Opal 690 (FP1497A) were used at a 1:1000 dilution in TSA buffer (#322809, ACD). RNAscope probes from ACD were used for the following targets: EPCAM (#418151), ENHO (#873251), LRG1 (#423381), LCN2 (#313971), HP (#532711), WNT4 (#401101), NRG4 (#493731), ADRB3 (#495521), UCP1 (#455411), and PPARGC1B (#402131). Slides were mounted with ProLong Diamond Antifade Mountant with DAPI (P36962, Life Technologies, Carlsbad, CA). Fluorescent signals were captured with the 40x objective lens on a laser scanning confocal microscope LSM880, (Zeiss, White Plains, NY).

Fluorescent-activated cell sorting (FACS)

Mammary gland white adipose tissue (mgWAT) from RT or cold exposed mice (Jackson Laboratory, #000664) was dissected, cut, and minced, and digested with collagenase D (5 mg/mL, #11088882001, Roche, Germany) and dispase (2 mg/mL, #17105041, Gibco, Grand Island, NY) over 40 min at 37°C with gentle shaking, 100 RPM. Enzymatic digestion was stopped with DMEM/15% FBS and the cell suspension was filtered through a 100 µm nylon mesh cell strainer, and centrifuged for 10 minutes at 700 x g. SVF pellet was resuspended in 1

mL Red Blood Cell lysis buffer (#41027700, Roche, Germany) and incubated for 5 minutes at room temperature. Cell suspension was diluted in 4 mL DPBS and filtered through a 40 µm nylon mesh cell strainer and centrifuged for 10 minutes at 700 x g. Single cell suspension was blocked for 10 minutes on ice in 500 µL DPBS/5% BSA (blocking buffer), centrifuged for 10 min at 700 x g, resuspended in 200 µL of DBPS/0.5% BSA (FACS buffer) solution containing the desired antibody mix, and incubated for 1 hour at 4°C in the dark with gentle rotation. Antibody-stained samples were washed with 800 µL FACS buffer, centrifuged 10 minutes at 700 x g, and resuspended in FACS buffer containing DAPI (at 1 ug/mL). Flow cytometry analysis was performed on a BD FACS Canto II (BD Biosciences, San Jose, CA) and results analyzed on FCS Express software (DeNovo Software, Pasadena, CA). Fluorescently-tagged anti-mouse antibodies (BioLegend, San Diego, CA) were used to label cell surface markers for flow cytometry analysis: EPCAM-FITC (clone G8.8, #118207), Sca-1-APC (Ly6, clone E13-161.7, #122512), CD49f-APC (clone GoH3, #313616). For flow cytometry analysis, negative selection of CD45-expressing cells using CD45 microbeads (#130052301) was performed immediately previous to the EPCAM positive selection protocol described above.

Isolation, selection, and *ex vivo* treatment of Epcam-positive cells

MACS microbeads (Miltenyi Biotec, Auburn, CA) were used for immuno-magnetic labeling positive selection of EPCAM-expressing cells (anti-CD326, #130105958). Before magnetic labeling, a single-cell suspension from the stromal vascular fraction of female mouse iWAT was prepared in MACS buffer, i.e. PBS, pH 7.2, 0.5% bovine serum albumin (#A7030, SIGMA, St. Louis, MO) and 2 mM EDTA, and filtered through a MACS pre-separation 30 µm nylon mesh

(#130041407) to remove cell clumps. Then, for magnetic labeling of EPCAM-expressing cells, 10 µL of EPCAM microbeads were added per $1x10^7$ total cells in 100 uL buffer, incubated for 15 minutes with rotation at 4°C, washed with 1 mL buffer, centrifuged at 700 x *g* for 5 minutes, resuspended in 500 µL buffer, and added to a pre-equilibrated MACS LS column (#130042401) in the magnetic field of a MACS separator (#130042302). Unlabeled EPCAM-negative cells were collected in the flow-through and three subsequent washes. The column was removed from the magnetic field, 5 mL of MACS buffer were added to the column, and the magnetically-labeled EPCAM-positive cells retained in the column were collected by flushing the cells down the column with a plunger. Finally, EPCAM-negative and EPCAM-positive cell populations were centrifuged at 700 x *g* for 5 minutes, resuspended in DMEM/F12 with glutamax supplemented with 15% FBS and 1% pen/strep (Thermo Scientific, CA) and plated on Collagen I-coated 12-well tissue culture plates (#354500, Corning, Kennebunk, ME). Media was replaced every other day during 6 days, followed by cell lysis with Tryzol for phenol/chloroform RNA extraction, and RT-qPCR analysis.

Adipocyte differentiation and treatments

10T1/2 or SVF from the 4th inguinal (iWAT) mgWAT isolated from 8 weeks old female *Lcn2*-null mice, respectively. 10T1/2 cells were maintained as previously described [55]. The pre-iWAT cells were maintained in Dulbecco's Modified Eagle Medium: Nutrient Mixture F-12 (DMEM/F12) supplemented with 1% glutamax, 10% fetal calf serum and 100 U/ml of both penicillin and streptomycin (basal media). Two days after plating (day 0), when the cells reached nearly 100% confluency, the cells were treated with an induction media containing basal media supplemented with 4 µg/mL insulin, 0.5 mM IBMX, 1 µM dexamethasone, and 1 µM rosiglitazone. After 48 h,

the cells were treated with a maintenance media containing the basal media supplemented with 4 μg/mL insulin, and 1 μM rosiglitazone, with a media change every 2 days until day 10. For qPCR, differentiated iWAT cells were treated with 1 μg/ml recombinant LCN2 (Sino Biological Inc.) or differentiated 10T1/2 cells were treated with LRG1 (R&D Systems) for 24 h and then treated with isoproterenol (Sigma) for 6 h after which RNA was collected.

CONFLICTS OF INTEREST

The authors declare no conflicts of interest.

REFERENCES

1 Chi, J. *et al.* Three-Dimensional Adipose Tissue Imaging Reveals Regional Variation in Beige Fat Biogenesis and PRDM16-Dependent Sympathetic Neurite Density. *Cell Metab* **27**, 226-236 e223, doi:10.1016/j.cmet.2017.12.011 (2018).

2 Schreiber, R. *et al.* Cold-Induced Thermogenesis Depends on ATGL-Mediated Lipolysis in Cardiac Muscle, but Not Brown Adipose Tissue. *Cell Metab* **26**, 753-763 e757, doi:10.1016/j.cmet.2017.09.004 (2017).

3 Gjorevski, N. & Nelson, C. M. Integrated morphodynamic signalling of the mammary gland. *Nat Rev Mol Cell Biol* **12**, 581-593, doi:10.1038/nrm3168 (2011).

4 McNally, S. & Martin, F. Molecular regulators of pubertal mammary gland development. *Ann Med* **43**, 212-234, doi:10.3109/07853890.2011.554425 (2011).

5 Inman, J. L., Robertson, C., Mott, J. D. & Bissell, M. J. Mammary gland development: cell fate specification, stem cells and the microenvironment. *Development* **142**, 1028-1042, doi:10.1242/dev.087643 (2015).

6 Wang, Q. A. & Scherer, P. E. Remodeling of Murine Mammary Adipose Tissue during Pregnancy, Lactation, and Involution. *J Mammary Gland Biol Neoplasia* **24**, 207-212, doi:10.1007/s10911-019-09434-2 (2019).

7 Landskroner-Eiger, S., Park, J., Israel, D., Pollard, J. W. & Scherer, P. E. Morphogenesis of the developing mammary gland: stage-dependent impact of adipocytes. *Dev Biol* **344**, 968-978, doi:10.1016/j.ydbio.2010.06.019 (2010).

8 Wang, Q. A. *et al.* Reversible De-differentiation of Mature White Adipocytes into Preadipocyte-like Precursors during Lactation. *Cell Metab* **28**, 282-288 e283, doi:10.1016/j.cmet.2018.05.022 (2018).

9 Lapid, K., Lim, A., Berglund, E. D. & Lu, Y. Estrogen receptor inhibition enhances cold-induced adipocyte beiging and glucose tolerance. *Diabetes Metab Syndr Obes* **12**, 1419-1436, doi:10.2147/DMSO.S190752 (2019).
10 Butler, A., Hoffman, P., Smibert, P., Papalexi, E. & Satija, R. Integrating single-cell transcriptomic data across different conditions, technologies, and species. *Nat Biotechnol* **36**, 411-420, doi:10.1038/nbt.4096 (2018).
11 Arneson, D. *et al.* Single cell molecular alterations reveal target cells and pathways of concussive brain injury. *Nat Commun* **9**, 3894, doi:10.1038/s41467-018-06222-0 (2018).
12 Bach, K. *et al.* Differentiation dynamics of mammary epithelial cells revealed by single-cell RNA sequencing. *Nat Commun* **8**, 2128, doi:10.1038/s41467-017-02001-5 (2017).
13 Tabula Muris, C. *et al.* Single-cell transcriptomics of 20 mouse organs creates a Tabula Muris. *Nature* **562**, 367-372, doi:10.1038/s41586-018-0590-4 (2018).
14 Tabula Muris, C. A single-cell transcriptomic atlas characterizes ageing tissues in the mouse. *Nature* **583**, 590-595, doi:10.1038/s41586-020-2496-1 (2020).
15 Li CM, S. H., Tsiobikas C, Selfors L, Chen H, Gray GK, Oren Y, Pinello L, Regev A, Brugge JS. Aging-associated alterations in the mammary gland revealed by single-cell RNA sequencing. *bioRxiv* (2019).
16 Burl, R. B. *et al.* Deconstructing Adipogenesis Induced by β3-Adrenergic Receptor Activation with Single-Cell Expression Profiling. *Cell Metabolism* **28**, 300-309.e304, doi:https://doi.org/10.1016/j.cmet.2018.05.025 (2018).
17 Tanaka, T., Yoshida, N., Kishimoto, T. & Akira, S. Defective adipocyte differentiation in mice lacking the C/EBPbeta and/or C/EBPdelta gene. *EMBO J* **16**, 7432-7443, doi:10.1093/emboj/16.24.7432 (1997).
18 Pei, H., Yao, Y., Yang, Y., Liao, K. & Wu, J. R. Kruppel-like factor KLF9 regulates PPARgamma transactivation at the middle stage of adipogenesis. *Cell Death Differ* **18**, 315-327, doi:10.1038/cdd.2010.100 (2011).
19 Kimura, H. & Fujimori, K. Activation of early phase of adipogenesis through Kruppel-like factor KLF9-mediated, enhanced expression of CCAAT/enhancer-binding protein beta in 3T3-L1 cells. *Gene* **534**, 169-176, doi:10.1016/j.gene.2013.10.065 (2014).
20 Siersbaek, R., Nielsen, R. & Mandrup, S. Transcriptional networks and chromatin remodeling controlling adipogenesis. *Trends Endocrinol Metab* **23**, 56-64, doi:10.1016/j.tem.2011.10.001 (2012).
21 Efremova, M., Vento-Tormo, M., Teichmann, S. A. & Vento-Tormo, R. CellPhoneDB: inferring cell-cell communication from combined expression of multi-subunit ligand-receptor complexes. *Nat Protoc* **15**, 1484-1506, doi:10.1038/s41596-020-0292-x (2020).
22 Rajbhandari, P. *et al.* Single cell analysis reveals immune cell-adipocyte crosstalk regulating the transcription of thermogenic adipocytes. *Elife* **8**, doi:10.7554/eLife.49501 (2019).
23 Jonker, J. W. *et al.* A PPARgamma-FGF1 axis is required for adaptive adipose remodelling and metabolic homeostasis. *Nature* **485**, 391-394, doi:10.1038/nature10998 (2012).
24 Regan, J. L. *et al.* c-Kit is required for growth and survival of the cells of origin of Brca1-mutation-associated breast cancer. *Oncogene* **31**, 869-883, doi:10.1038/onc.2011.289 (2012).
25 Visvader, J. E. & Stingl, J. Mammary stem cells and the differentiation hierarchy: current status and perspectives. *Genes Dev* **28**, 1143-1158, doi:10.1101/gad.242511.114 (2014).

26 Brisken, C. *et al.* Essential function of Wnt-4 in mammary gland development downstream of progesterone signaling. *Genes Dev* **14**, 650-654 (2000).
27 Robinson, G. W. & Hennighausen, L. Inhibins and activins regulate mammary epithelial cell differentiation through mesenchymal-epithelial interactions. *Development* **124**, 2701-2708 (1997).
28 Aryal, B. *et al.* Absence of ANGPTL4 in adipose tissue improves glucose tolerance and attenuates atherogenesis. *JCI Insight* **3**, doi:10.1172/jci.insight.97918 (2018).
29 De Keyser, J., De Backer, J. P., Ebinger, G. & Vauquelin, G. Regional distribution of the dopamine D2 receptors in the mesotelencephalic dopamine neuron system of human brain. *J Neurol Sci* **71**, 119-127, doi:10.1016/0022-510x(85)90041-3 (1985).
30 Arner, E. *et al.* Ceruloplasmin is a novel adipokine which is overexpressed in adipose tissue of obese subjects and in obesity-associated cancer cells. *PLoS One* **9**, e80274, doi:10.1371/journal.pone.0080274 (2014).
31 Chella Krishnan, K. *et al.* Sex-specific metabolic functions of adipose Lipocalin-2. *Mol Metab* **30**, 30-47, doi:10.1016/j.molmet.2019.09.009 (2019).
32 Sun, W. Y. *et al.* Lipocalin-2 derived from adipose tissue mediates aldosterone-induced renal injury. *JCI Insight* **3**, doi:10.1172/jci.insight.120196 (2018).
33 Deis, J. A. *et al.* Adipose Lipocalin 2 overexpression protects against age-related decline in thermogenic function of adipose tissue and metabolic deterioration. *Mol Metab* **24**, 18-29, doi:10.1016/j.molmet.2019.03.007 (2019).
34 Ishii, A. *et al.* Obesity-promoting and anti-thermogenic effects of neutrophil gelatinase-associated lipocalin in mice. *Sci Rep* **7**, 15501, doi:10.1038/s41598-017-15825-4 (2017).
35 Wang, G. X. *et al.* The brown fat-enriched secreted factor Nrg4 preserves metabolic homeostasis through attenuation of hepatic lipogenesis. *Nat Med* **20**, 1436-1443, doi:10.1038/nm.3713 (2014).
36 Maffei, M., Barone, I., Scabia, G. & Santini, F. The Multifaceted Haptoglobin in the Context of Adipose Tissue and Metabolism. *Endocr Rev* **37**, 403-416, doi:10.1210/er.2016-1009 (2016).
37 Kumar, K. G. *et al.* Identification of adropin as a secreted factor linking dietary macronutrient intake with energy homeostasis and lipid metabolism. *Cell Metab* **8**, 468-481, doi:10.1016/j.cmet.2008.10.011 (2008).
38 Gargiulo, L. *et al.* A Novel Effect of beta-Adrenergic Receptor on Mammary Branching Morphogenesis and its Possible Implications in Breast Cancer. *J Mammary Gland Biol Neoplasia* **22**, 43-57, doi:10.1007/s10911-017-9371-1 (2017).
39 Marchetti, B. *et al.* Beta-adrenergic receptors in the rat mammary gland during pregnancy and lactation: characterization, distribution, and coupling to adenylate cyclase. *Endocrinology* **126**, 565-574, doi:10.1210/endo-126-1-565 (1990).
40 Nedvetsky, P. I., Kwon, S. H., Debnath, J. & Mostov, K. E. Cyclic AMP regulates formation of mammary epithelial acini in vitro. *Mol Biol Cell* **23**, 2973-2981, doi:10.1091/mbc.E12-02-0078 (2012).
41 Aibar, S. *et al.* SCENIC: single-cell regulatory network inference and clustering. *Nat Methods* **14**, 1083-1086, doi:10.1038/nmeth.4463 (2017).
42 Oakes, S. R. *et al.* The Ets transcription factor Elf5 specifies mammary alveolar cell fate. *Genes Dev* **22**, 581-586, doi:10.1101/gad.1614608 (2008).
43 Street, K. *et al.* Slingshot: cell lineage and pseudotime inference for single-cell transcriptomics. *BMC Genomics* **19**, 477, doi:10.1186/s12864-018-4772-0 (2018).

44 Khalifeh-Soltani, A. *et al.* Mfge8 promotes obesity by mediating the uptake of dietary fats and serum fatty acids. *Nat Med* **20**, 175-183, doi:10.1038/nm.3450 (2014).
45 Bauters, D., Van Hul, M. & Lijnen, H. R. Macrophage elastase (MMP-12) in expanding murine adipose tissue. *Biochim Biophys Acta* **1830**, 2954-2959, doi:10.1016/j.bbagen.2012.12.024 (2013).
46 Lee, J. T. *et al.* Macrophage metalloelastase (MMP12) regulates adipose tissue expansion, insulin sensitivity, and expression of inducible nitric oxide synthase. *Endocrinology* **155**, 3409-3420, doi:10.1210/en.2014-1037 (2014).
47 Shao, M. *et al.* Zfp423 Maintains White Adipocyte Identity through Suppression of the Beige Cell Thermogenic Gene Program. *Cell Metab* **23**, 1167-1184, doi:10.1016/j.cmet.2016.04.023 (2016).
48 Gavalda-Navarro, A. *et al.* Lipopolysaccharide-binding protein is a negative regulator of adipose tissue browning in mice and humans. *Diabetologia* **59**, 2208-2218, doi:10.1007/s00125-016-4028-y (2016).
49 Sun, W. *et al.* snRNA-seq reveals a subpopulation of adipocytes that regulates thermogenesis. *Nature* **587**, 98-102, doi:10.1038/s41586-020-2856-x (2020).
50 Kiefer, F. W. *et al.* Retinaldehyde dehydrogenase 1 regulates a thermogenic program in white adipose tissue. *Nat Med* **18**, 918-925, doi:10.1038/nm.2757 (2012).
51 Guilherme, A. *et al.* Control of Adipocyte Thermogenesis and Lipogenesis through beta3-Adrenergic and Thyroid Hormone Signal Integration. *Cell Rep* **31**, 107598, doi:10.1016/j.celrep.2020.107598 (2020).
52 Dobin, A. *et al.* STAR: ultrafast universal RNA-seq aligner. *Bioinformatics* **29**, 15-21, doi:10.1093/bioinformatics/bts635 (2013).
53 Kim, D., Langmead, B. & Salzberg, S. L. HISAT: a fast spliced aligner with low memory requirements. *Nat Methods* **12**, 357-360, doi:10.1038/nmeth.3317 (2015).
54 Love, M. I., Anders, S., Kim, V. & Huber, W. RNA-Seq workflow: gene-level exploratory analysis and differential expression. *F1000Res* **4**, 1070, doi:10.12688/f1000research.7035.1 (2015).
55 Rajbhandari, P. *et al.* IL-10 Signaling Remodels Adipose Chromatin Architecture to Limit Thermogenesis and Energy Expenditure. *Cell* **172**, 218-233 e217, doi:10.1016/j.cell.2017.11.019 (2018).
56 Hafemeister, C. & Satija, R. Normalization and variance stabilization of single-cell RNA-seq data using regularized negative binomial regression. *Genome Biology* **20**, 296, doi:10.1186/s13059-019-1874-1 (2019).
57 Butler, A., Hoffman, P., Smibert, P., Papalexi, E. & Satija, R. Integrating single-cell transcriptomic data across different conditions, technologies, and species. *Nature Biotechnology* **36**, 411-420, doi:10.1038/nbt.4096 (2018).
58 Stuart, T. *et al.* Comprehensive Integration of Single-Cell Data. *Cell* **177**, 1888-1902.e1821, doi:10.1016/j.cell.2019.05.031 (2019).
59 McInnes, L., Healy, J. & Melville, J. UMAP: Uniform Manifold Approximation and Projection for Dimension Reduction. *arXiv* (2018).
60 van der Maaten, L. & Hinton, G. Visualizing Data using t-SNE. *J Mach Learn Res*, 2579-2605 (2008).
61 Blondel, V. D., Guillaume, J.-L., Lambiotte, R. & Lefebvre, E. Fast unfolding of communities in large networks. *Journal of Statistical Mechanics: Theory and Experiment* **2008**, P10008, doi:10.1088/1742-5468/2008/10/P10008 (2008).

62 Broad Institute. *Study: Mouse Adipose Stromal Vascular Fraction*, <https://singlecell.broadinstitute.org/single_cell/study/SCP708/mouse-adipose-stromal-vascular-fraction#study-summary> (

63 Bach, K. *et al.* Differentiation dynamics of mammary epithelial cells revealed by single-cell RNA sequencing. *Nature Communications* **8**, 2128, doi:10.1038/s41467-017-02001-5 (2017).

64 Guo, G. MCA DGE Data. *Figshare*, doi:10.6084/m9.figshare.5435866.v8 (2020).

65 Han, X. *et al.* Mapping the Mouse Cell Atlas by Microwell-Seq. *Cell* **172**, 1091-1107.e1017, doi:10.1016/j.cell.2018.02.001 (2018).

66 Tabula Muris: Transcriptomic characterization of 20 organs and tissues from Mus musculus at single cell resolution.

67 Tabula Muris Senis.

68 Kanehisa, M. & Goto, S. KEGG: Kyoto Encyclopedia of Genes and Genomes. *Nucleic Acids Research* **28**, 27-30, doi:10.1093/nar/28.1.27 (2000).

69 Jassal, B. *et al.* The Reactome Pathway Knowledgebase. *Nucleic Acids Research* **48**, D498-D503, doi:10.1093/nar/gkz1031 (2020).

70 Nishimura, D. BioCarta. *Biotech Software & Internet Report* **2**, 117-120, doi:10.1089/152791601750294344 (2001).

71 Ashburner, M. *et al.* Gene Ontology: tool for the unification of biology. *Nature Genetics* **25**, 25-29, doi:10.1038/75556 (2000).

72 Saelens, W., Cannoodt, R., Todorov, H. & Saeys, Y. A comparison of single-cell trajectory inference methods. *Nature Biotechnology* **37**, 547-554, doi:10.1038/s41587-019-0071-9 (2019).

73 Van de Sande, B. *et al.* A scalable SCENIC workflow for single-cell gene regulatory network analysis. *Nature Protocols* **15**, 2247-2276, doi:10.1038/s41596-020-0336-2 (2020).

74 Moerman, T. *et al.* GRNBoost2 and Arboreto: efficient and scalable inference of gene regulatory networks. *Bioinformatics* **35**, 2159-2161, doi:10.1093/bioinformatics/bty916 (2019).

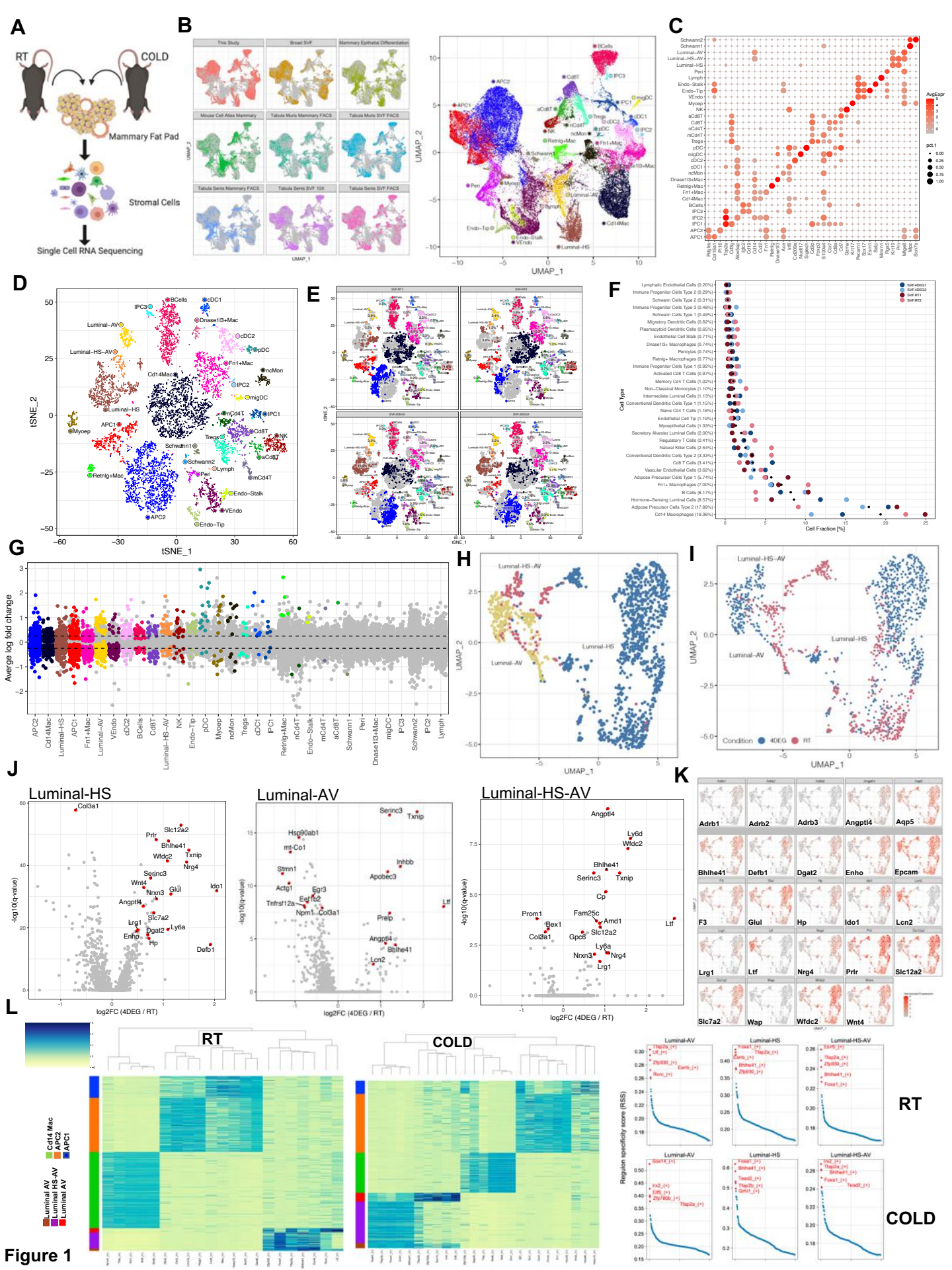
A
RT
COLD
Mammary Fat Pad
Stromal Cells
Single Cell RNA Sequencing
B
This Study
Broad SVF
Mammary Epithelial Differentiation
Mouse Cell Atlas Mammary
Tabula Muris Mammary FACS
Tabula Muris SVF FACS
Tabula Senis Mammary FACS
Tabula Senis SVF 10X
Tabula Senis SVF FACS
UMAP_1
UMAP_2
C
AvgExpr
pct.1
D
tSNE_1
tSNE_2
E
F
Cell Type
Cell Fraction [%]
G
Averge log fold change
H
I
Condition
4DEG
RT
J
Luminal-HS
Luminal-AV
Luminal-HS-AV
log2FC (4DEG / RT)
-log10(q-value)
K
L
RT
COLD
Regulon specificity score (RSS)
Figure 1

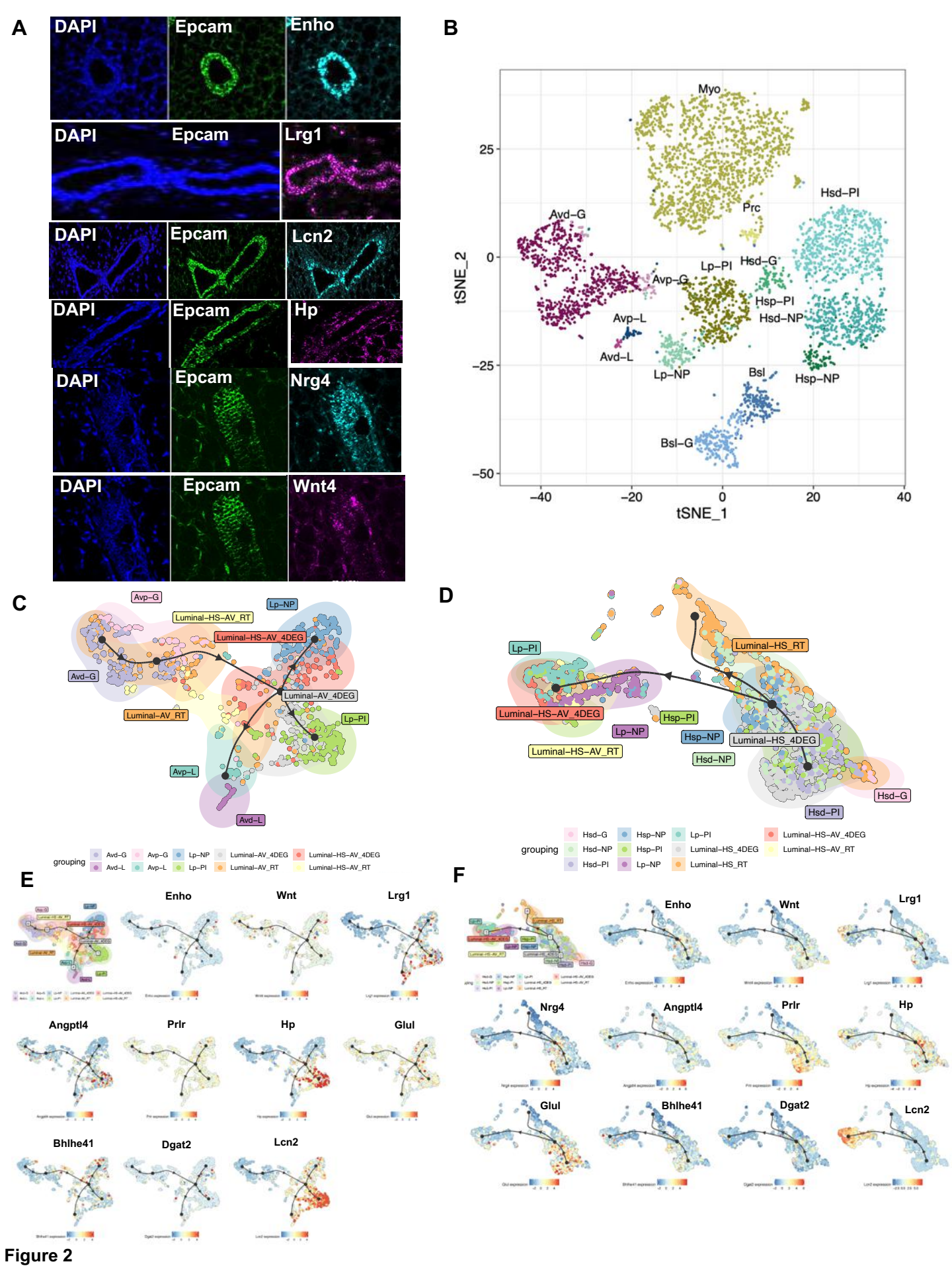
A
DAPI
Epcam
Enho
Lrg1
Lcn2
Hp
Nrg4
Wnt4
B
Myo
Prc
Hsd−PI
Avd−G
Lp−PI
Hsd−G
Avp−G
Hsp−PI
Hsd−NP
Avp−L
Avd−L
Lp−NP
Bsl
Hsp−NP
Bsl−G
tSNE_2
tSNE_1
C
Avp−G
Lp−NP
Luminal−HS−AV_RT
Luminal−HS−AV_4DEG
Avd−G
Luminal−AV_4DEG
Luminal−AV_RT
Lp−PI
Avp−L
Avd−L
grouping
Avd−G
Avd−L
Avp−G
Avp−L
Lp−NP
Lp−PI
Luminal−AV_4DEG
Luminal−AV_RT
Luminal−HS−AV_4DEG
Luminal−HS−AV_RT
D
Lp−PI
Luminal−HS_RT
Luminal−HS−AV_4DEG
Hsp−PI
Lp−NP
Hsp−NP
Luminal−HS_4DEG
Luminal−HS−AV_RT
Hsd−NP
Hsd−G
Hsd−PI
grouping
Hsd−G
Hsd−NP
Hsd−PI
Hsp−NP
Hsp−PI
Lp−NP
Lp−PI
Luminal−HS_4DEG
Luminal−HS_RT
Luminal−HS−AV_4DEG
Luminal−HS−AV_RT
E
Enho
Wnt
Lrg1
Angptl4
Prlr
Hp
Glul
Bhlhe41
Dgat2
Lcn2
F
Enho
Wnt
Lrg1
Nrg4
Angptl4
Prlr
Hp
Glul
Bhlhe41
Dgat2
Lcn2

Figure 2

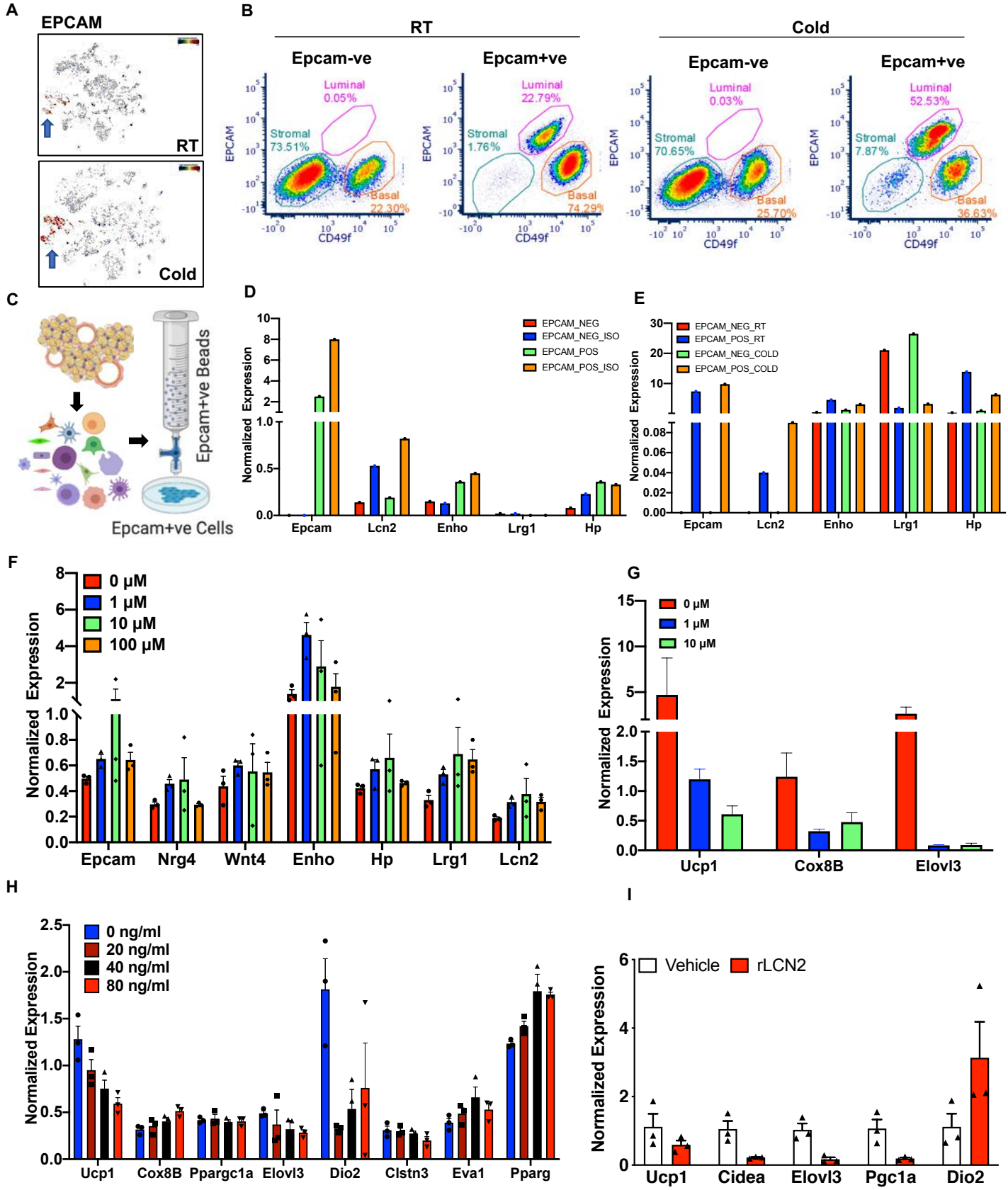
A
EPCAM
RT
Cold
B
RT
Cold
Epcam-ve
Epcam+ve
Epcam-ve
Epcam+ve
Luminal 0.05%
Stromal 73.51%
Basal 22.30%
Luminal 22.79%
Stromal 1.76%
Basal 74.29%
Luminal 0.03%
Stromal 70.65%
Basal 25.70%
Luminal 52.53%
Stromal 7.87%
Basal 36.63%
EPCAM
CD49f
C
Epcam+ve Beads
Epcam+ve Cells
D
EPCAM_NEG
EPCAM_NEG_ISO
EPCAM_POS
EPCAM_POS_ISO
Normalized Expression
Epcam
Lcn2
Enho
Lrg1
Hp
E
EPCAM_NEG_RT
EPCAM_POS_RT
EPCAM_NEG_COLD
EPCAM_POS_COLD
Normalized Expression
Epcam
Lcn2
Enho
Lrg1
Hp
F
0 μM
1 μM
10 μM
100 μM
Normalized Expression
Epcam
Nrg4
Wnt4
Enho
Hp
Lrg1
Lcn2
G
0 μM
1 μM
10 μM
Normalized Expression
Ucp1
Cox8B
Elovl3
H
0 ng/ml
20 ng/ml
40 ng/ml
80 ng/ml
Normalized Expression
Ucp1
Cox8B
Ppargc1a
Elovl3
Dio2
Clstn3
Eva1
Pparg
I
Vehicle
rLCN2
Normalized Expression
Ucp1
Cidea
Elovl3
Pgc1a
Dio2

Figure 3

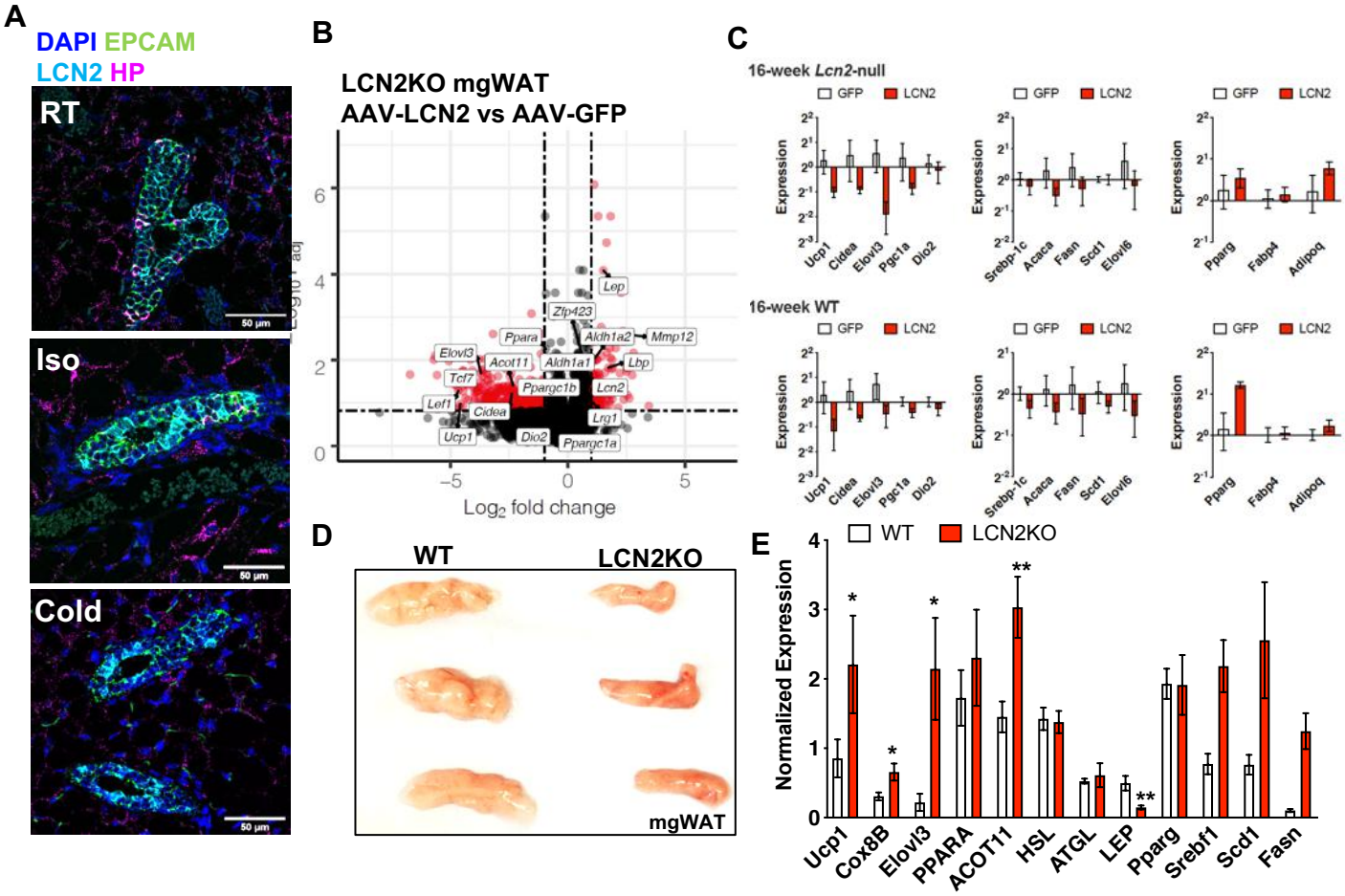
A
DAPI EPCAM
LCN2 HP
RT
Iso
Cold
50 µm
B
LCN2KO mgWAT
AAV-LCN2 vs AAV-GFP
Log10 Padj
Log2 fold change
Lep
Zfp423
Ppara
Aldh1a2
Mmp12
Elovl3
Acot11
Aldh1a1
Lbp
Tcf7
Ppargc1b
Lcn2
Lef1
Cidea
Lrg1
Ucp1
Dio2
Ppargc1a
C
16-week Lcn2-null
16-week WT
GFP
LCN2
Expression
Ucp1
Cidea
Elovl3
Pgc1a
Dio2
Srebp-1c
Acaca
Fasn
Scd1
Elovl6
Pparg
Fabp4
Adipoq
D
WT
LCN2KO
mgWAT
E
WT
LCN2KO
Normalized Expression
Ucp1
Cox8B
Elovl3
PPARA
ACOT11
HSL
ATGL
LEP
Pparg
Srebf1
Scd1
Fasn

Figure 4

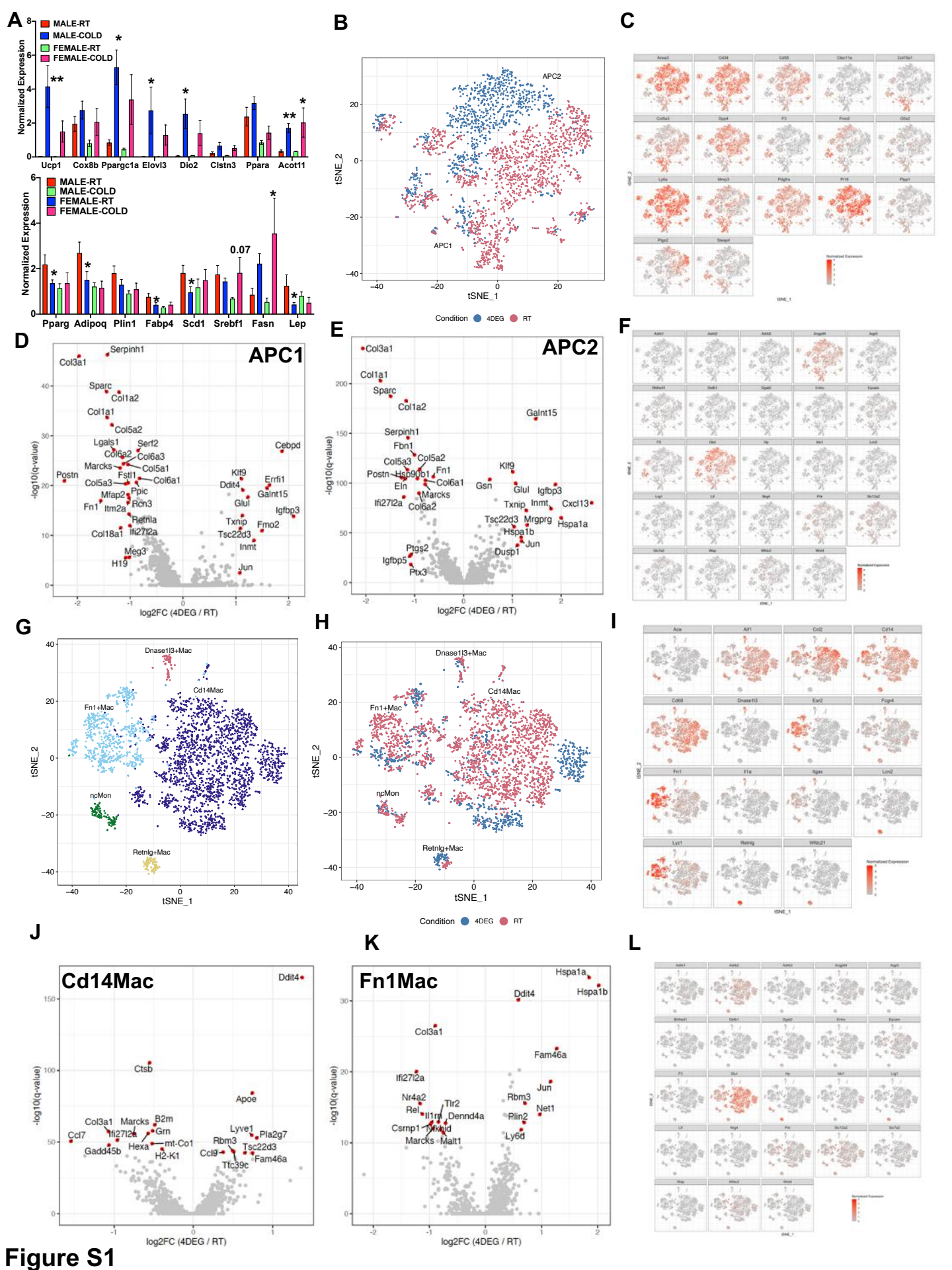
A
MALE-RT
MALE-COLD
FEMALE-RT
FEMALE-COLD
Normalized Expression
Ucp1
Cox8b
Ppargc1a
Elovl3
Dio2
Clstn3
Ppara
Acot11
Pparg
Adipoq
Plin1
Fabp4
Scd1
Srebf1
Fasn
Lep
0.07
B
APC1
APC2
tSNE_1
tSNE_2
Condition
4DEG
RT
C
D
APC1
Serpinh1
Col3a1
Sparc
Col1a2
Col1a1
Col5a2
Lgals1
Serf2
Col6a2
Col6a3
Cebpd
Marcks
Col5a1
Postn
Fstl1
Col6a1
Klf9
Ddit4
Errfi1
Col5a3
Ppic
Galnt15
Mfap2
Rcn3
Glul
Igfbp3
Fn1
Itm2a
Retnla
Txnip
Fmo2
Col18a1
Ifi27l2a
Tsc22d3
Inmt
Meg3
H19
Jun
log2FC (4DEG / RT)
-log10(q-value)
E
APC2
Col3a1
Col1a1
Sparc
Col1a2
Galnt15
Serpinh1
Fbn1
Col5a2
Col5a3
Fn1
Postn
Hsp90b1
Klf9
Eln
Col6a1
Gsn
Glul
Igfbp3
Marcks
Ifi27l2a
Col6a2
Txnip
Inmt
Cxcl13
Tsc22d3
Mrgprg
Hspa1a
Hspa1b
Jun
Ptgs2
Dusp1
Igfbp5
Ptx3
F
G
Dnase1l3+Mac
Cd14Mac
Fn1+Mac
ncMon
Retnlg+Mac
tSNE_1
tSNE_2
H
Dnase1l3+Mac
Cd14Mac
Fn1+Mac
ncMon
Retnlg+Mac
Condition
4DEG
RT
I
J
Cd14Mac
Ddit4
Ctsb
Apoe
Col3a1
Marcks
B2m
Grn
Ccl7
Ifi27l2a
Hexa
mt-Co1
Gadd45b
H2-K1
Rbm3
Lyve1
Pla2g7
Ccl9
Tsc22d3
Ttc39c
Fam46a
log2FC (4DEG / RT)
-log10(q-value)
K
Fn1Mac
Hspa1a
Hspa1b
Ddit4
Col3a1
Fam46a
Ifi27l2a
Jun
Nr4a2
Tlr2
Rbm3
Net1
Rel
Il1rn
Dennd4a
Plin2
Csrnp1
Nfkbid
Ly6d
Marcks
Malt1
log2FC (4DEG / RT)
-log10(q-value)
L

Figure S1

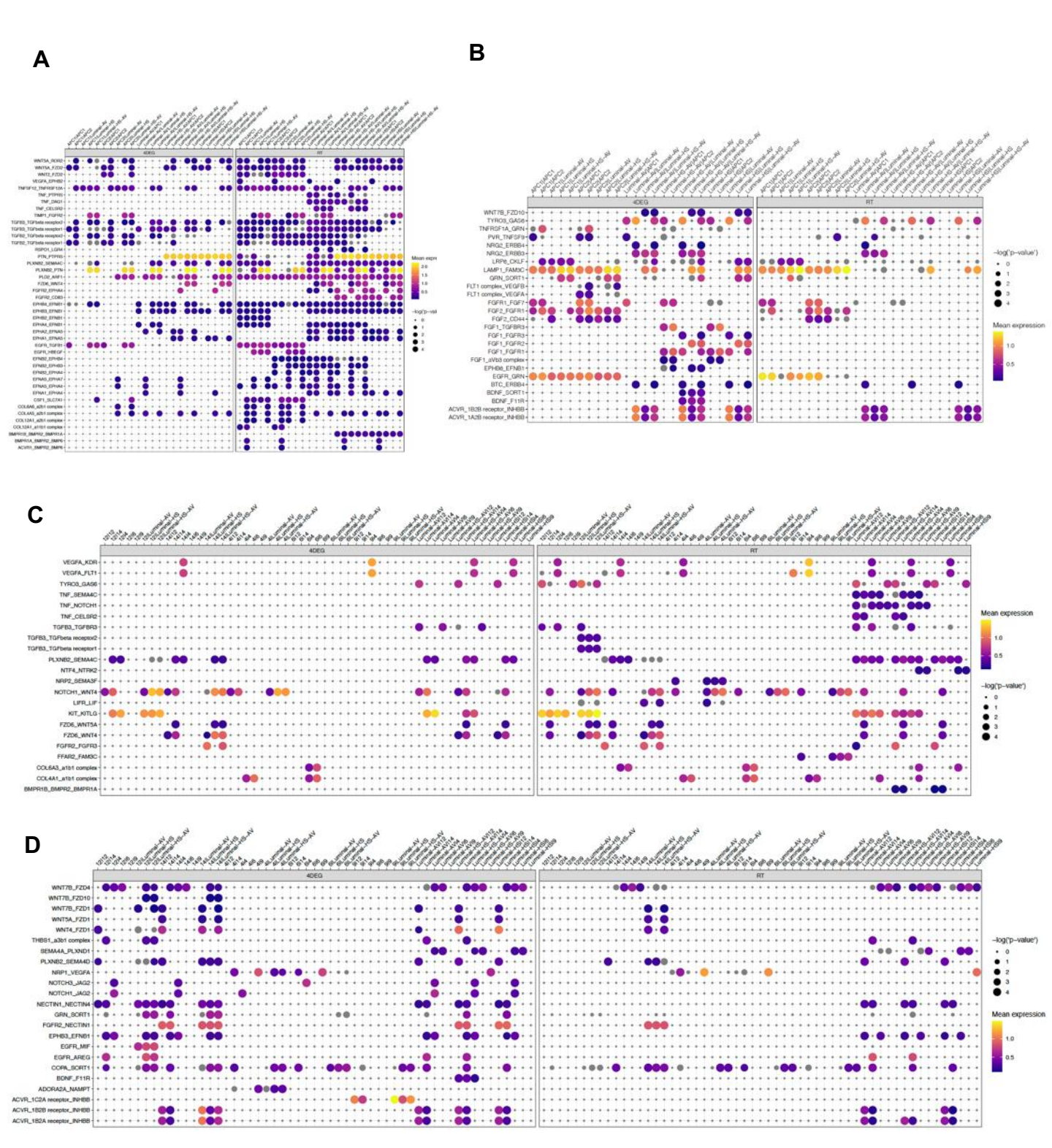

Figure S2

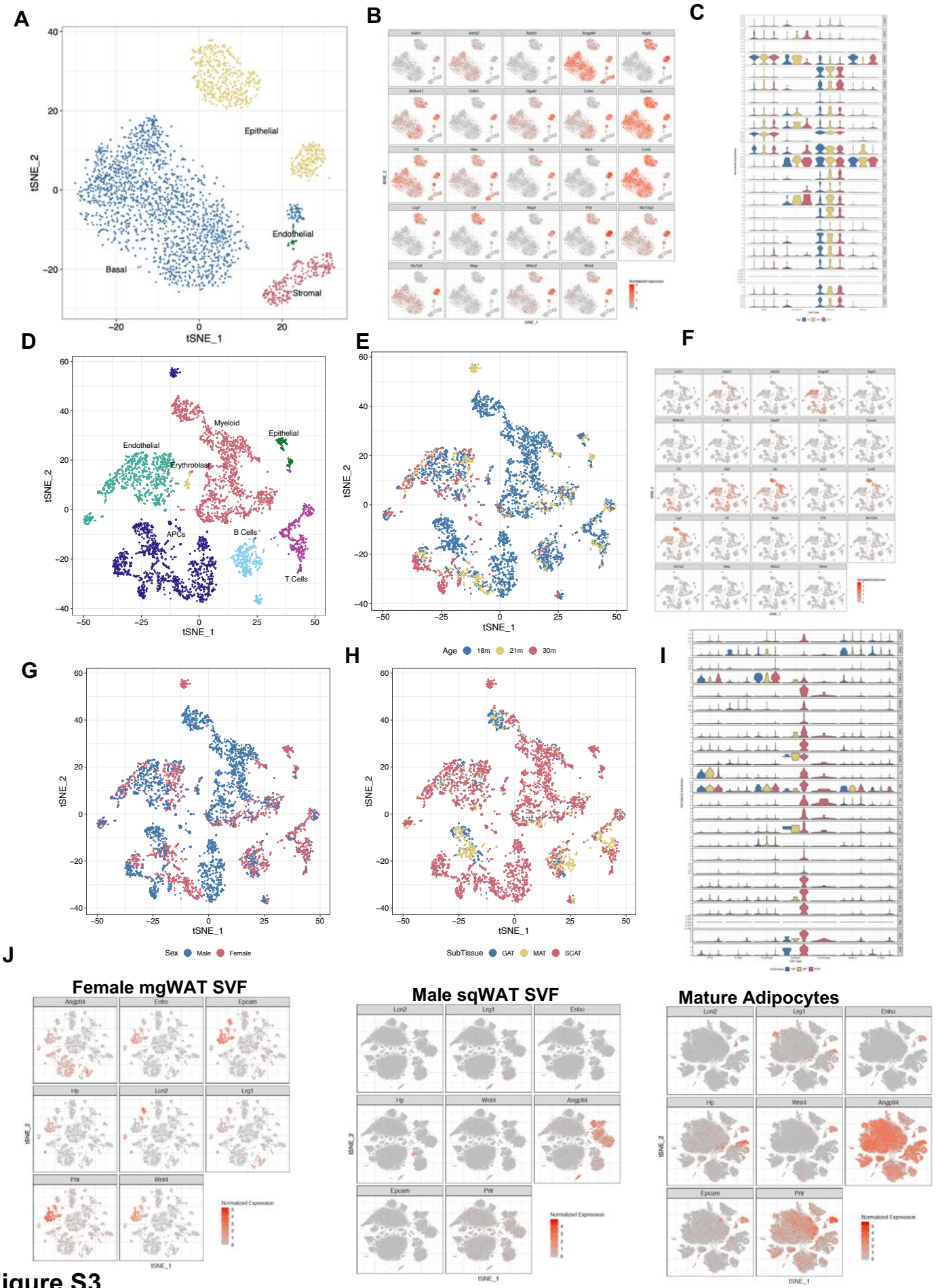
A
Epithelial
Endothelial
Basal
Stromal
tSNE_1
tSNE_2
B
C
D
Myeloid
Epithelial
Endothelial
Erythroblast
APCs
B Cells
T Cells
E
Age 18m 21m 30m
F
G
Sex Male Female
H
SubTissue GAT MAT SCAT
I
J
Female mgWAT SVF
Male sqWAT SVF
Mature Adipocytes
Normalized Expression

Figure S3

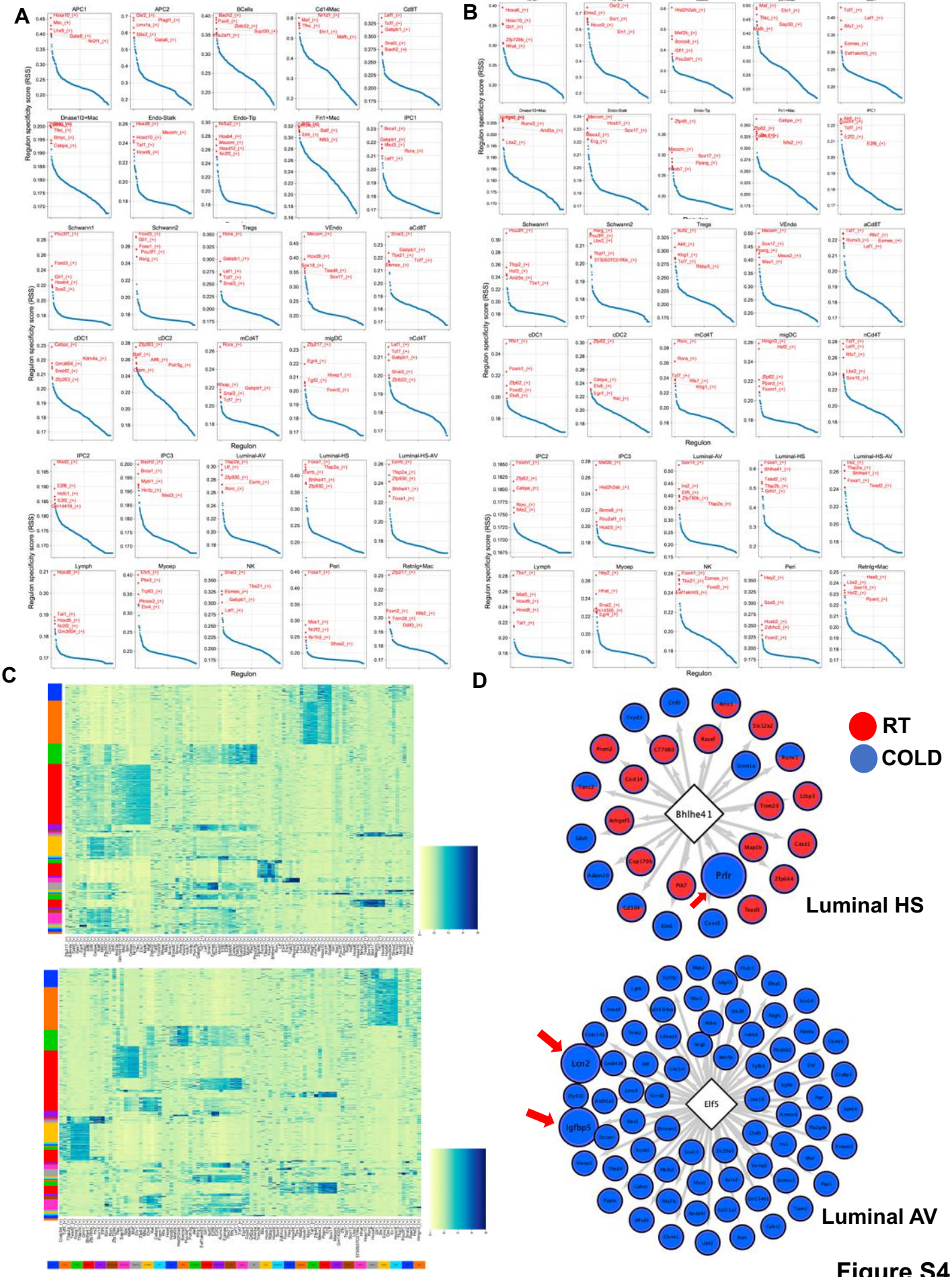
A
B
C
D
Regulon specificity score (RSS)
Regulon
APC1
APC2
BCells
Cd14Mac
Cd8T
Dnase1l3+Mac
Endo-Stalk
Endo-Tip
Fn1+Mac
IPC1
Schwann1
Schwann2
Tregs
VEndo
aCd8T
cDC1
cDC2
mCd4T
migDC
nCd4T
IPC2
IPC3
Luminal-AV
Luminal-HS
Luminal-HS-AV
Lymph
Myoep
NK
Peri
Retnlg+Mac
RT
COLD
Bhlhe41
Prlr
Luminal HS
Elf5
Lcn2
Igfbp5
Luminal AV

Figure S4

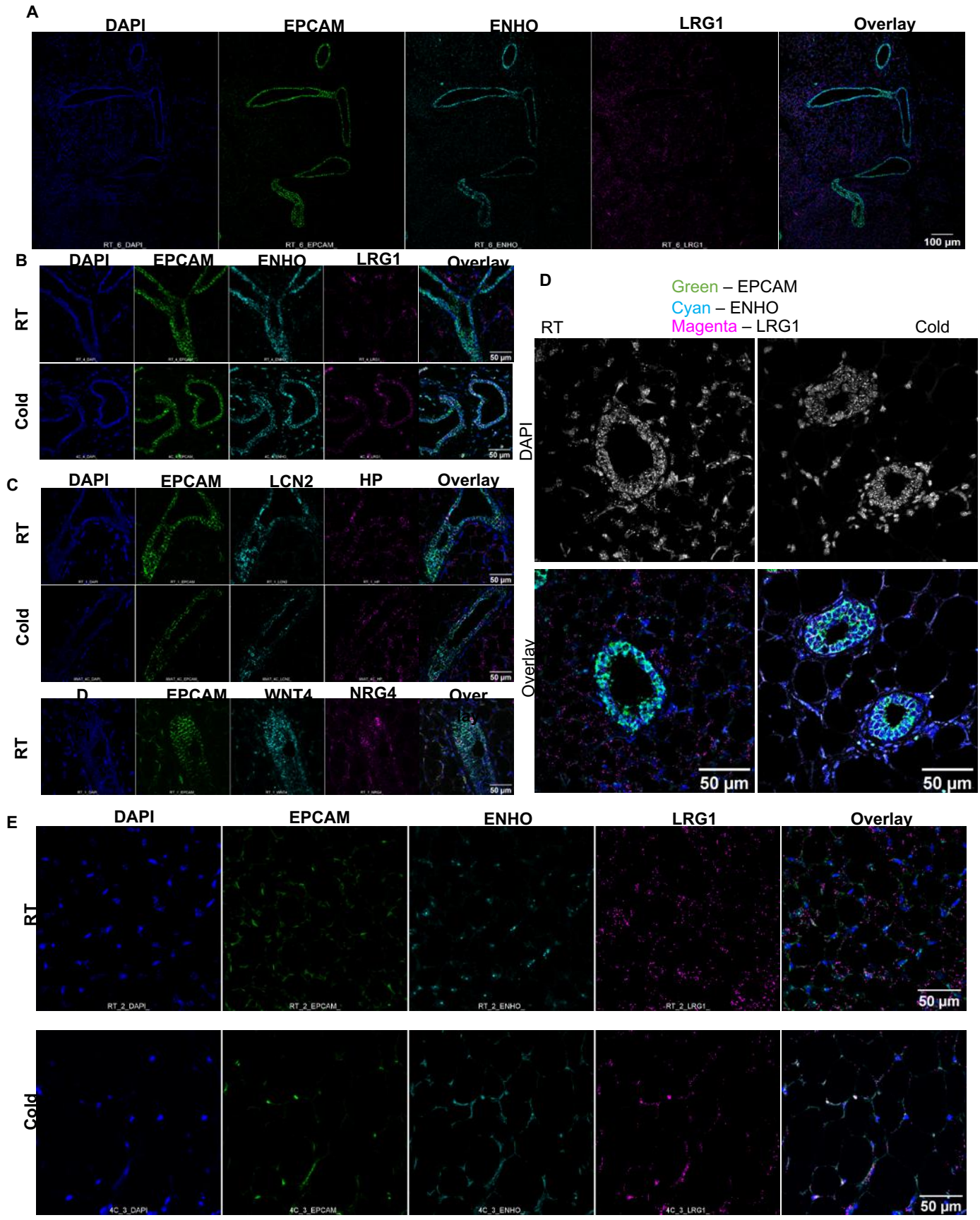
A
DAPI
EPCAM
ENHO
LRG1
Overlay
100 µm
B
DAPI
EPCAM
ENHO
LRG1
Overlay
RT
Cold
50 µm
C
DAPI
EPCAM
LCN2
HP
Overlay
RT
Cold
50 µm
D
EPCAM
WNT4
NRG4
RT
50 µm
D
Green – EPCAM
Cyan – ENHO
Magenta – LRG1
RT
Cold
DAPI
Overlay
50 µm
50 µm
E
DAPI
EPCAM
ENHO
LRG1
Overlay
RT
Cold
50 µm
50 µm

Figure S5

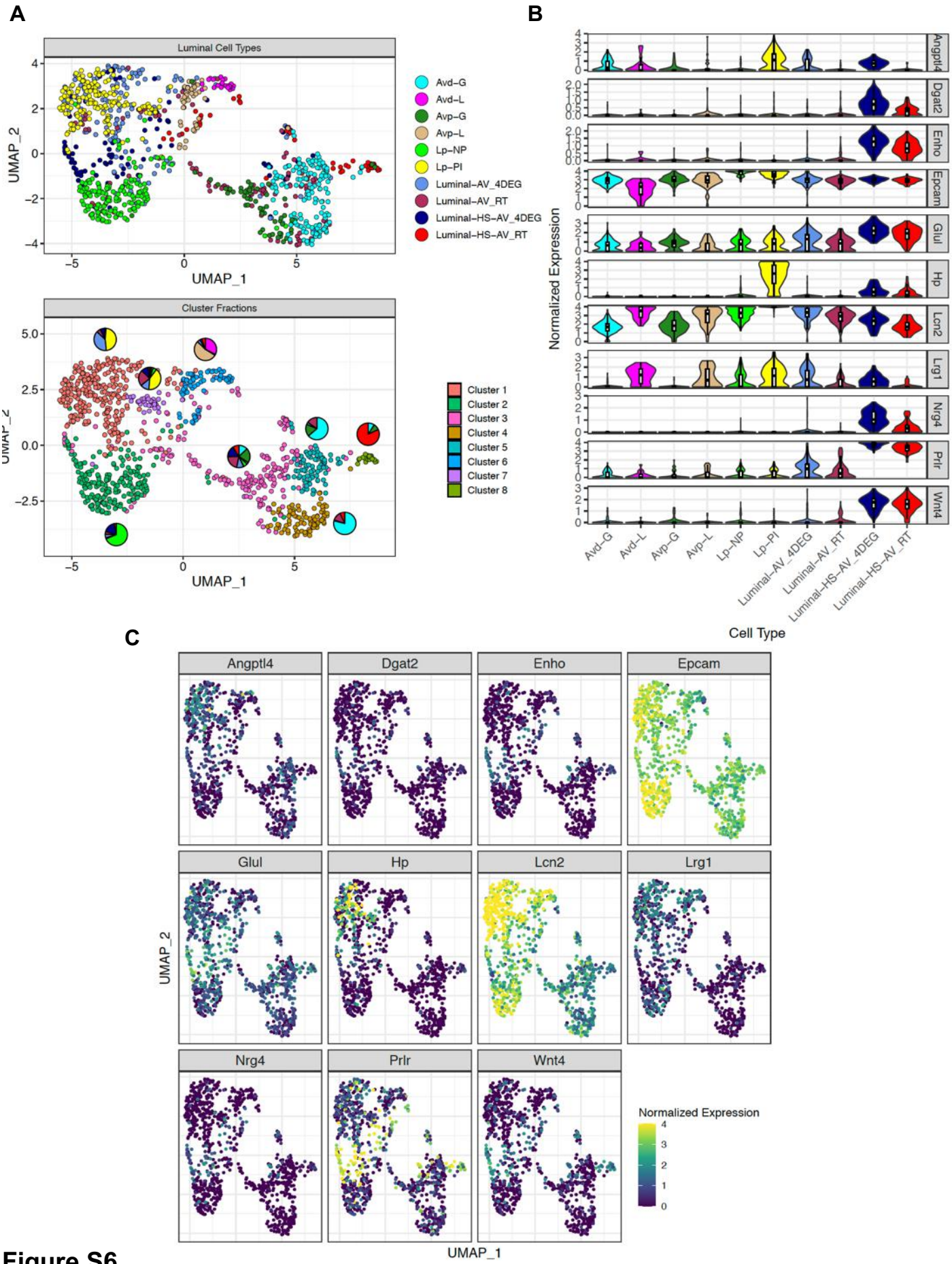
A
Luminal Cell Types
UMAP_2
UMAP_1
Avd–G
Avd–L
Avp–G
Avp–L
Lp–NP
Lp–PI
Luminal–AV_4DEG
Luminal–AV_RT
Luminal–HS–AV_4DEG
Luminal–HS–AV_RT
Cluster Fractions
Cluster 1
Cluster 2
Cluster 3
Cluster 4
Cluster 5
Cluster 6
Cluster 7
Cluster 8
B
Angptl4
Dgat2
Enho
Epcam
Glul
Hp
Lcn2
Lrg1
Nrg4
Prlr
Wnt4
Normalized Expression
Cell Type
C
Angptl4
Dgat2
Enho
Epcam
Glul
Hp
Lcn2
Lrg1
Nrg4
Prlr
Wnt4
UMAP_2
UMAP_1
Normalized Expression

Figure S6

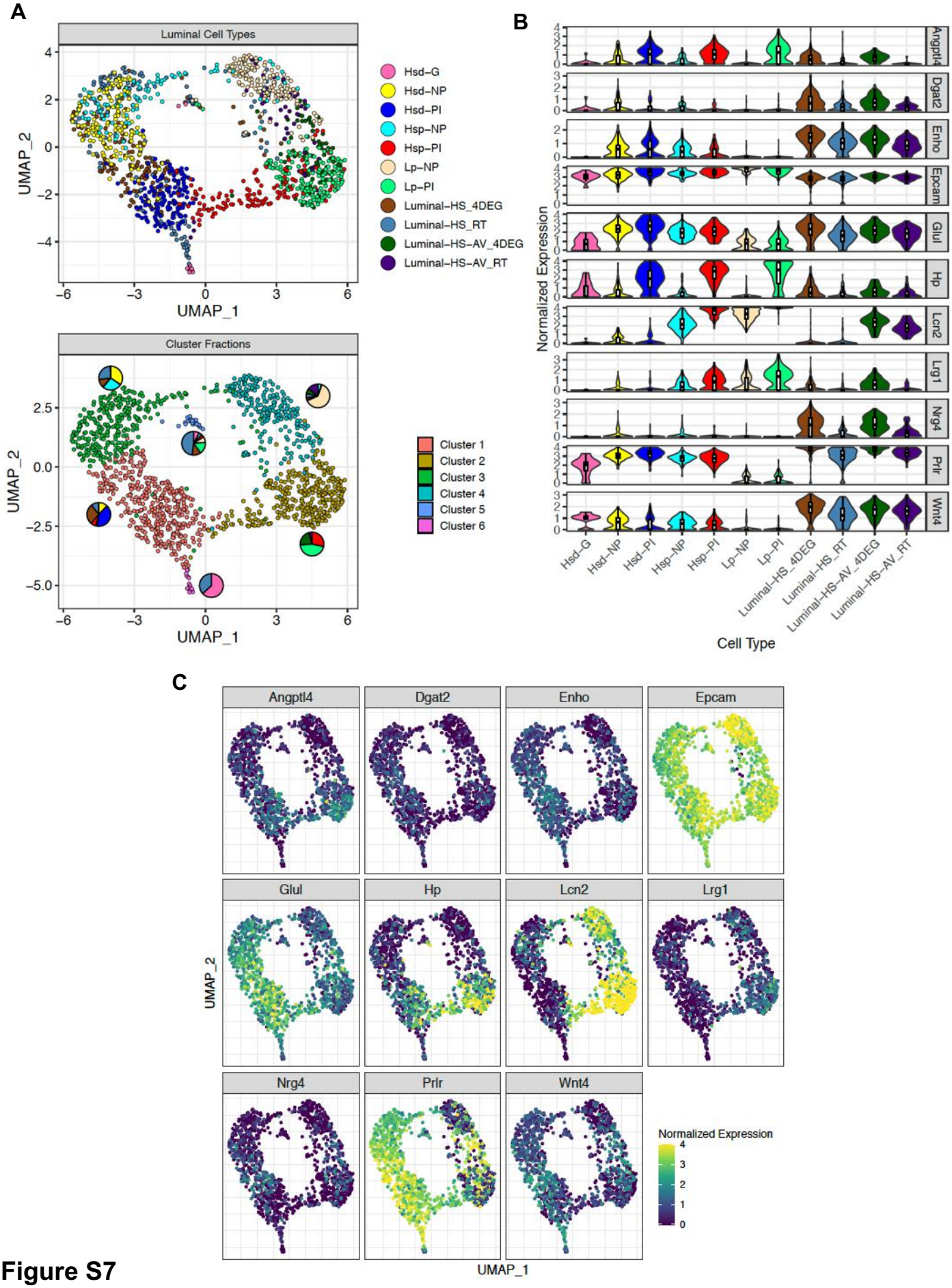
A
Luminal Cell Types
UMAP_2
UMAP_1
Hsd−G
Hsd−NP
Hsd−PI
Hsp−NP
Hsp−PI
Lp−NP
Lp−PI
Luminal−HS_4DEG
Luminal−HS_RT
Luminal−HS−AV_4DEG
Luminal−HS−AV_RT
Cluster Fractions
Cluster 1
Cluster 2
Cluster 3
Cluster 4
Cluster 5
Cluster 6
B
Angptl4
Dgat2
Enho
Epcam
Glul
Hp
Lcn2
Lrg1
Nrg4
Prlr
Wnt4
Normalized Expression
Cell Type
C
Normalized Expression

Figure S7

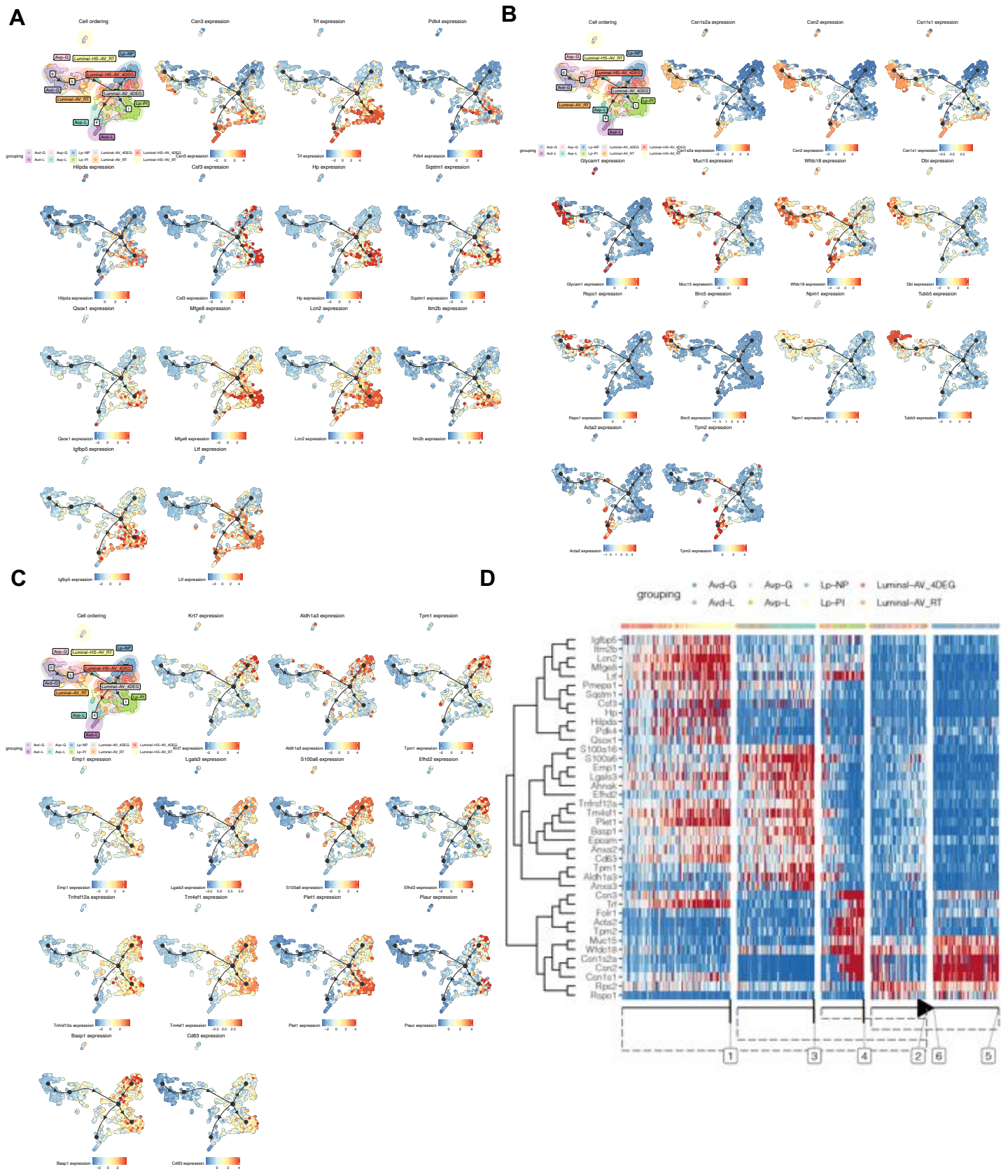
A
B
C
D
Cell ordering
grouping
Avd-G
Avd-L
Avp-G
Avp-L
Lp-NP
Lp-PI
Luminal-AV_4DEG
Luminal-AV_RT
Luminal-HS-AV_4DEG
Luminal-HS-AV_RT
Hilpda expression
Csf3 expression
Hp expression
Sqstm1 expression
Qsox1 expression
Mfge8 expression
Lcn2 expression
Itm2b expression
Igfbp5 expression
Ltf expression
Glycam1 expression
Muc15 expression
Wfdc18 expression
Dbi expression
Rspo1 expression
Birc5 expression
Npm1 expression
Tubb5 expression
Acta2 expression
Tpm2 expression
Krt7 expression
Aldh1a3 expression
Tpm1 expression
Emp1 expression
Lgals3 expression
S100a6 expression
Efhd2 expression
Tnfrsf12a expression
Tm4sf1 expression
Plet1 expression
Plaur expression
Basp1 expression
Cd63 expression
Igfbp5
Itm2b
Lcn2
Mfge8
Ltf
Pmepa1
Sqstm1
Csf3
Hp
Hilpda
Pdk4
Qsox1
S100a16
S100a6
Emp1
Lgals3
Ahnak
Efhd2
Tnfrsf12a
Tm4sf1
Plet1
Basp1
Epcam
Anxa2
Cd63
Tpm1
Aldh1a3
Anxa3
Csn3
Trf
Folr1
Acta2
Tpm2
Muc15
Wfdc18
Csn1s2a
Csn2
Csn1s1
Rpc2
Rspo1
1
3
4
2
6
5

Figure S8

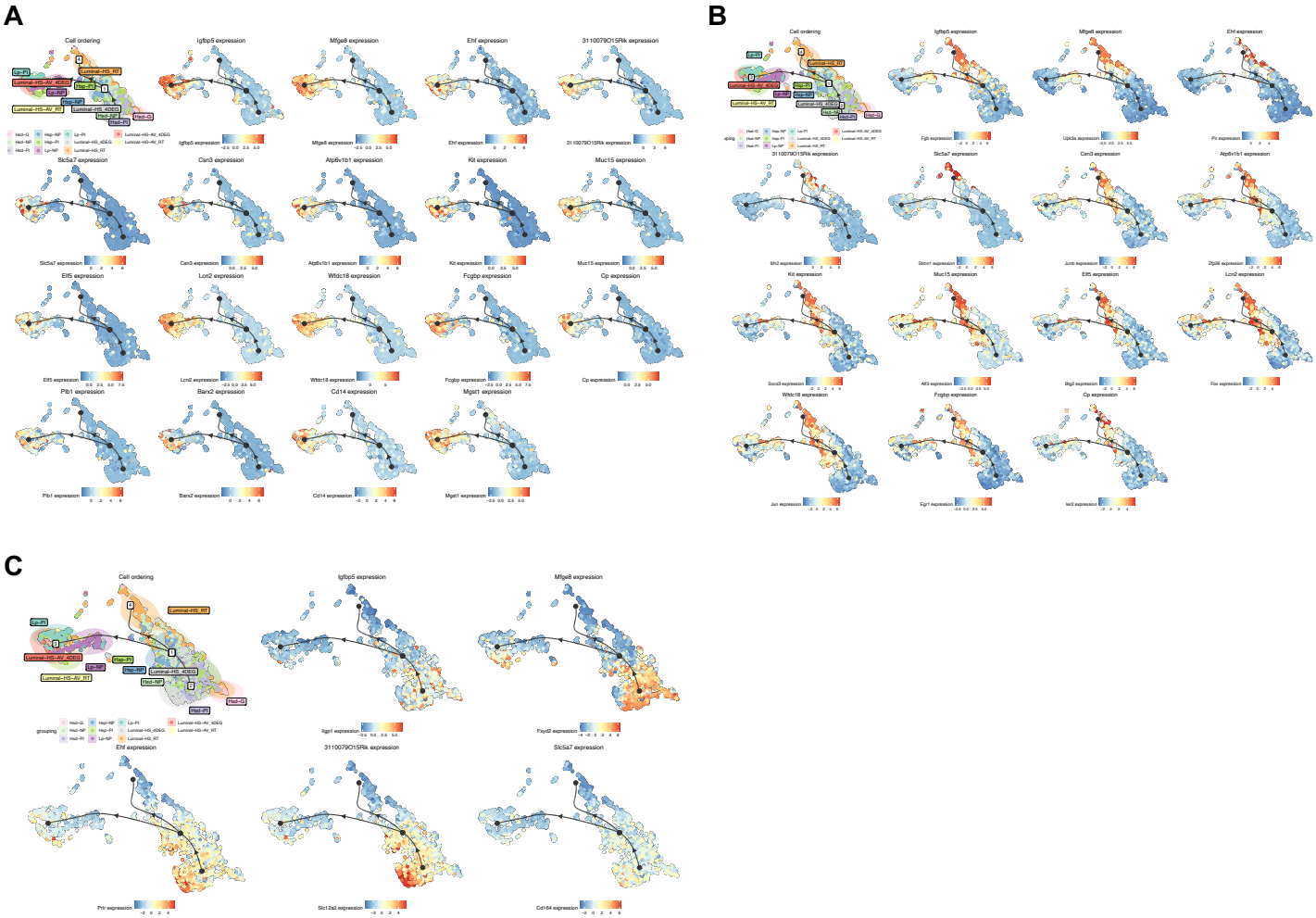
A
B
C
Cell ordering
Igfbp5 expression
Mfge8 expression
Ehf expression
3110079O15Rik expression
Slc5a7 expression
Car3 expression
Atp6v1b1 expression
Kit expression
Muc15 expression
Elf5 expression
Lcn2 expression
Wfdc18 expression
Fcgbp expression
Cp expression
Pltb1 expression
Barx2 expression
Cd14 expression
Mgst1 expression
Itih2 expression
Stmn1 expression
Junb expression
Zfp36 expression
Socs3 expression
Atf3 expression
Btg2 expression
Fos expression
Jun expression
Egr1 expression
Ier2 expression
Upk3a expression
Pir expression
Fgb expression
Ifgp1 expression
Fxyd2 expression
Slc12a2 expression
Cd164 expression
grouping
Hsd−G
Hsd−NP
Hsd−PI
Hsp−NP
Hsp−PI
Lp−NP
Lp−PI
Luminal−HS_4DEG
Luminal−HS_RT
Luminal−HS−AV_4DEG
Luminal−HS−AV_RT

D

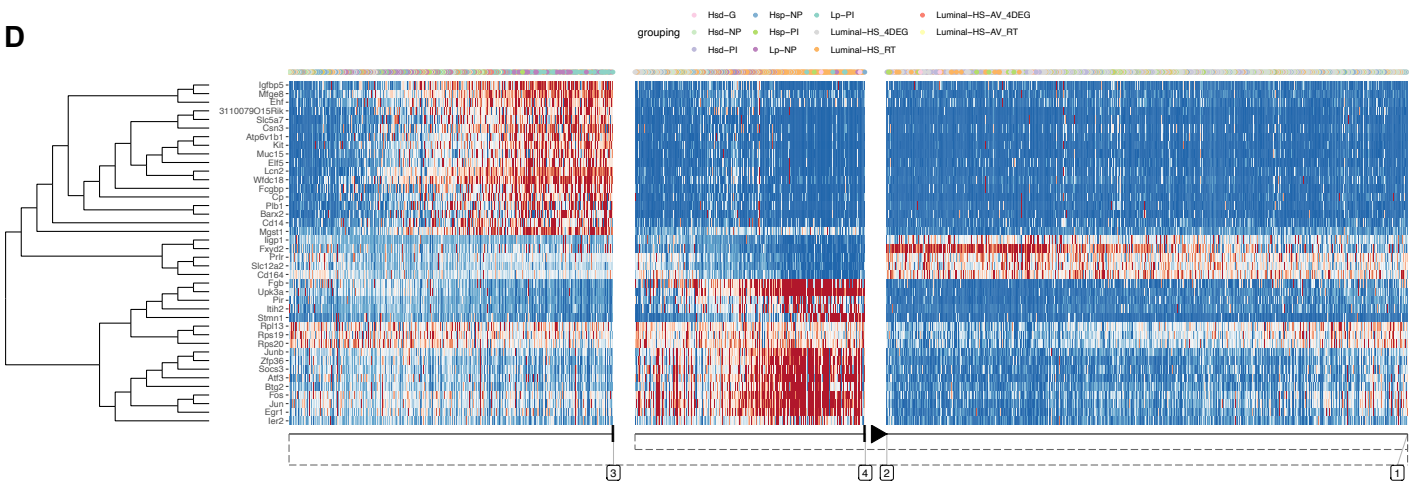
grouping
Hsd−G
Hsd−NP
Hsd−PI
Hsp−NP
Hsp−PI
Lp−NP
Lp−PI
Luminal−HS_4DEG
Luminal−HS_RT
Luminal−HS−AV_4DEG
Luminal−HS−AV_RT
Igfbp5
Mfge8
Ehf
3110079O15Rik
Slc5a7
Car3
Atp6v1b1
Kit
Muc15
Elf5
Lcn2
Wfdc18
Fcgbp
Cp
Pltb1
Barx2
Cd14
Mgst1
Ifgp1
Fxyd2
Pir
Slc12a2
Cd164
Fgb
Upk3a
Pir
Itih2
Stmn1
Rpl13
Rps19
Rps20
Junb
Zfp36
Socs3
Atf3
Btg2
Fos
Jun
Egr1
Ier2
3
4
2
1

Figure S9

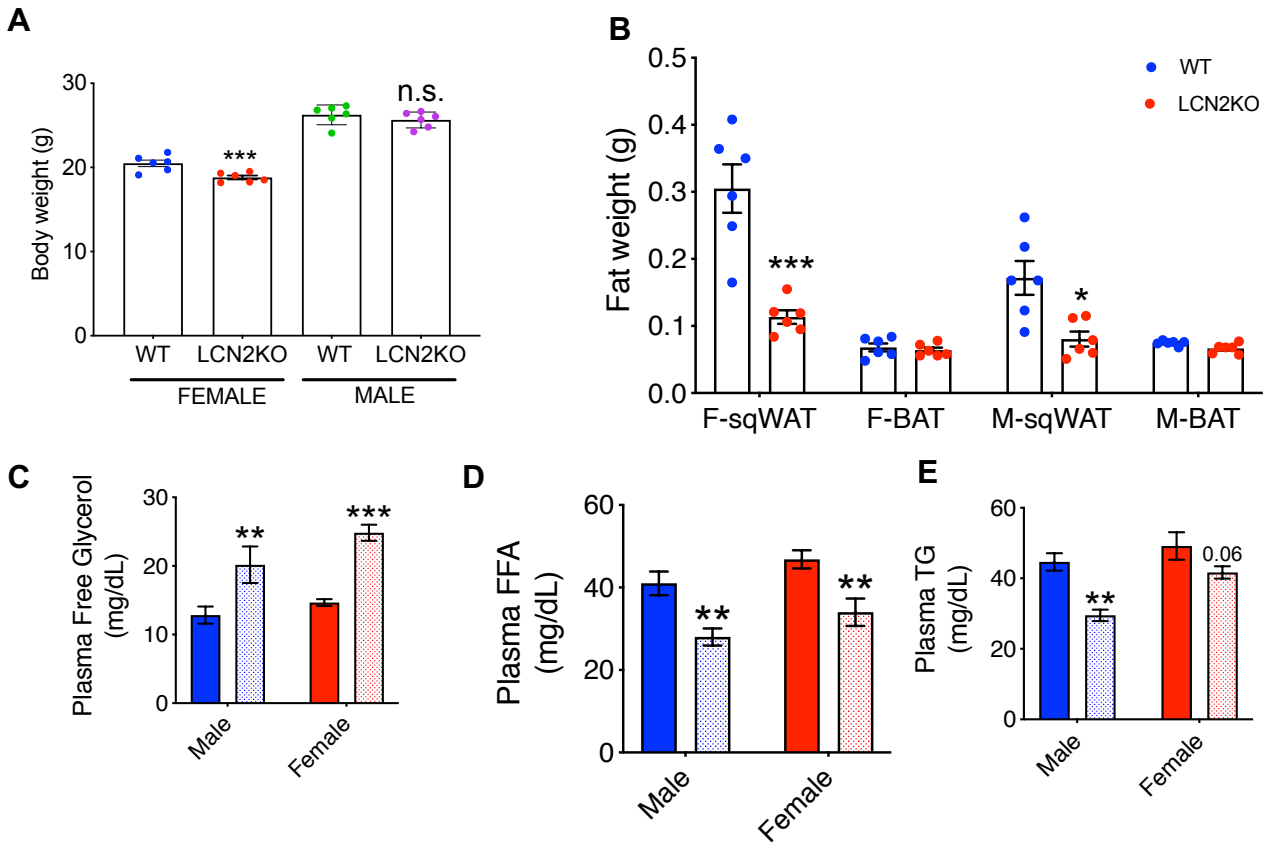
A
Body weight (g)
30
20
10
0
***
n.s.
WT
LCN2KO
WT
LCN2KO
FEMALE
MALE
B
Fat weight (g)
0.5
0.4
0.3
0.2
0.1
0.0
WT
LCN2KO
***
*
F-sqWAT
F-BAT
M-sqWAT
M-BAT
C
Plasma Free Glycerol (mg/dL)
30
20
10
0
**
***
Male
Female
D
Plasma FFA (mg/dL)
60
40
20
0
**
**
Male
Female
E
Plasma TG (mg/dL)
60
40
20
0
**
0.06
Male
Female

Figure S10